BIOCHEMISTRY
including biophysical chemistry & molecular biology

Article

pubs.acs.org/biochemistry

Functional Consequences of the Creation of an Asp-His-Fe Triad in a 3/3 Globin

Edward L. D'Antonio, Jennifer D'Antonio, Vesna de Serrano, Hanna Gracz, Matthew K. Thompson, Reza A. Ghiladi, Edmond F. Bowden,* and Stefan Franzen*

Department of Chemistry, North Carolina State University, Raleigh, North Carolina 27695-8204, United States

Supporting Information

ABSTRACT: The proximal side of dehaloperoxidase-hemoglobin A (DHP A) from *Amphitrite ornata* has been modified via site-directed mutagenesis of methionine 86 into aspartate (M86D) to introduce an Asp-His-Fe triad charge relay. X-ray crystallographic structure determination of the metcyano forms of M86D [Protein Data Bank (PDB) entry 3MYN] and M86E (PDB entry 3MYM) mutants reveal the structural origins of a stable catalytic triad in DHP A. A decrease in the rate of H_2O_2 activation as well as a lowered reduction potential versus that of the wild-type enzyme was observed in M86D. One possible explanation for the significantly lower activity is an increased affinity for the distal histidine in binding to the heme Fe to form a bis-histidine adduct. Resonance Raman spectroscopy demonstrates a pH-dependent ligation by the distal histidine in M86D, which is indicative of an increased trans effect. At pH 5.0, the heme Fe is five-coordinate, and this structure resembles the wild-type DHP A resting state. However, at pH 7.0, the distal histidine appears to form a six-coordinate ferric bis-histidine (hemichrome) adduct. These observations can be explained by the effect of the increased positive charge on the heme Fe on the formation of a six-coordinate low-spin adduct, which inhibits the ligation and activation of H_2O_2 as required for peroxidase activity. The results suggest that the proximal charge relay in peroxidases regulate the redox potential of the heme Fe but that the trans effect is a carefully balanced property that can both activate H_2O_2 and attract ligation by the distal histidine. To understand the balance of forces that modulate peroxidase reactivity, we studied three M86 mutants, M86A, M86D, and M86E, by spectroelectrochemistry and nuclear magnetic resonance spectroscopy of ^{13}C- and ^{15}N-labeled cyanide adducts as probes of the redox potential and of the trans effect in the heme Fe, both of which can be correlated with the proximity of negative charge to the N_δ hydrogen of the proximal histidine, consistent with an Asp-His-Fe charge relay observed in heme peroxidases.

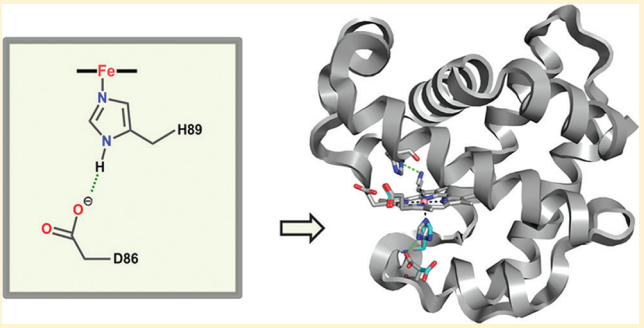

Dehaloperoxidase-hemoglobin A (DHP A) is an intracellular coelomic hemoglobin from the terebellid polychaete *Amphitrite ornata*.[1−3] In the presence of hydrogen peroxide, DHP A catalyzes the oxidative dehalogenation of substrate 2,4,6-tribromophenolate (TBP) to 2,6-dibromoquinone (DBQ).[4] DHP A can also dehalogenate other 2,4,6-trihalophenolates (TXPs) of like structure into their corresponding 2,6-dihaloquinones (DXQs). Although its 3-over-3 α-helical structural fold bears a close resemblance to the structures of mammalian globins,[5,6] DHP A was shown to have substantially higher peroxidase reactivity than the prototypical example, horse heart myoglobin (HHMb).[4]

The result of H_2O_2 binding to an Fe(III) peroxidase is a Compound 0 intermediate that subsequently undergoes O−O bond cleavage, as shown in Scheme 1.[7] We propose that these same mechanistic steps occur upon binding of H_2O_2 to the ferric form of DHP A, in accord with the peroxide reactivity observed in myoglobin.[8,9] The O−O bond cleavage that occurs in the DHP isoenzymes in the absence of substrate TXP results in the formation of Compound I, observed by cryoreduction,[10] which interconverts to Compound ES (Cpd ES), an Fe(IV)−

Scheme 1. Two-Electron Oxidation of Ferric DHP A to Compound ES That Is Initiated by Binding of Hydrogen Peroxide to the Heme Fe

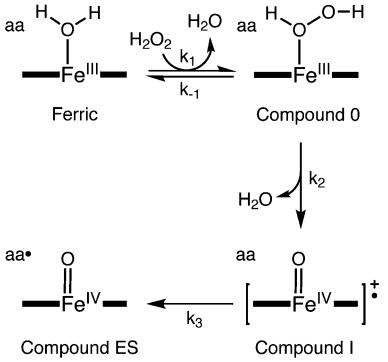

Received: August 30, 2011
Published: September 27, 2011

ferryl intermediate with a tyrosine radical, observed by rapid freeze quench methods.[11,12] Activation of bound H_2O_2 for O−O bond cleavage is a key step in peroxidase reactivity. The rate constant for the bond cleavage step (k_2) has been determined to be 3.56×10^4 M^{-1} s^{-1} for DHP A at pH 7.0.[11] In comparison, values on the order of 10^2 M^{-1} s^{-1} have been reported for globins, whereas peroxidases have rate constants on the order of $\sim 10^7$ M^{-1} s^{-1}.[9]

H_2O_2 activation in peroxidases has been mechanistically interpreted in terms of the "push−pull" effect.[13] The "push" effect refers to either proximal side ligands[14] or structure[15,16] that controls the amount of electron density that is pushed onto the heme Fe, whereas the "pull" effect results from distal side acid/base catalysis and/or stabilization of developing negative charge on the heme Fe-bound H_2O_2.[7,13] The essential need for the electron density push has been demonstrated by a mutation of wild-type cytochrome *c* peroxidase (C*c*P) in which the proximal histidine was replaced with glycine, i.e., H175G.[17] As a result of this mutation, a 4 order of magnitude decrease in the O−O bond cleavage rate occurs. Partial restoration of the wild-type O−O bond cleavage rate was observed upon diffusing exogenous imidazole into the proximal cavity to ligate the heme iron. Together, these results clearly demonstrated the essential role played by the proximal histidine in donating electron density to the heme Fe for peroxidase activation.

Redox control in peroxidases is apparently regulated by a charge relay that may serve as a functional determinant of the substrate range. Electrochemical studies of C*c*P, for example, have established that the presence of the Asp-His-Fe triad lowers its Fe(III)/Fe(II) reduction potential by ca. 100 mV relative to that of a mutant that lacks the triad.[14] On the basis of this study and other observations, it appears that the catalytic triad is important in stabilizing the higher oxidation states of the heme Fe in peroxidases.[18] The idea that the Asp-His-Fe catalytic triad may regulate the redox potential has gained further attention in a recent comparative study of peroxidases, in which the ability to oxidize substituted phenols was found to be dependent upon the Cpd II/Fe(III) reduction potential.[19] For example, nitrophenol is not oxidized by horseradish peroxidase [$E^{\circ}_{\text{Cpd II/Fe(III)}} = 0.89$ V] but is oxidized by *Coprinus cinereus* peroxidase (CiP) [$E^{\circ}_{\text{Cpd II/Fe(III)}} = 1.18$ V] and *Bjerkandera adusta* versatile peroxidase (VP) [$E^{\circ}_{\text{Cpd II/Fe(III)}} = 1.37$ V]. A correlation between the reduction potentials of the Fe(III)/Fe(II) and Cpd II/Fe(III) redox couples was also found. These observations suggest that peroxidases have evolved a means for redox tuning that is specific for their function.

The importance of secondary push effects such as hydrogen bonding that arise from interactions due to heme Fe second-shell ligands has been questioned in a commentary by Poulos,[16] especially in the case of the Asp-His-Fe triad in C*c*P. The Asp-His-Fe triad is a structural motif found in peroxidases that was proposed to be the basis of a principal push effect contribution[13] due to the influence of strong charge-mediated hydrogen bonding that leads to a charge relay. The charge relay involves the partial deprotonation of the proximal histidine N_δ hydrogen by strong hydrogen bonding to the aspartate residue. The partial negative charge on the proximal histidine was hypothesized to increase the basicity of N_ε, which ligates to the heme Fe. The increase in negative charge would in turn support a greater positive charge on the heme Fe. It was later determined, however, to play only a minor role in the rate of O−O bond cleavage when H_2O_2 reacts with C*c*P.[17,20] Elimination of the carboxylate−histidine hydrogen bonding interaction in C*c*P(D235N) produced only a minor decrease in the catalytic rate.[21] This observation leaves open the possibility that second-shell ligands involved in the push effect can still be considered important contributors for H_2O_2 activation. As a consequence, the role played by the Asp-His-Fe charge relay triad in peroxidase catalysis remains unclear. Although apparently not absolutely required for H_2O_2 activation, the triad may nevertheless serve to modulate the rate constant for H_2O_2 activation or the redox potential of the heme.[14] Redox modulation affects the substrate range accessible to peroxidase oxidations. A charge relay (either Asp-His-Fe or Glu-His-Fe) is found in every peroxidase, yet such charge relays are absent from globins with the exception of flavohemoglobins.[22,23,24]

Protein engineering studies have failed to produce a stable globin mutant capable of accommodating a buried negative charge in a proximal side triad structure. Replacement of S92 with aspartate in mammalian myoglobins, such as SWMb-(S92D)[25] and HHMb(S92D/T67R),[26] gave rise to proteins having the aspartate negative charge oriented away from the proximal histidine and toward the bulk solvent. The L89D mutant of SWMb was reported as a proximal charge relay,[27] but the instability of this mutant made it unsuitable for engineering studies[28] and precluded characterization by X-ray crystallography. The proximal structure in DHP A has been observed to give rise to an Fe−His interaction that is stronger than those in other globins.[29,30] DHP A lacks the proximal region serine residue typically observed in myoglobins, and the proximal histidine (H89) maintains a hydrogen bond with the backbone carbonyl of L83. There is also a methionine residue (M86) near H89, for which the $(M86)S_\delta-(H89)N_\delta$ separation ranges between 3.5 and 4.4 Å [Protein Data Bank (PDB) entry 2QFK]; however, there are no obvious strong interactions between these residues.

The unique bifunctional nature of DHP A suggests that the proximal side may be capable of stabilizing charge in a manner that differs from that of other globins. To test this hypothesis, we sought to create proximal mutations that would yield an Asp-His-Fe triad and/or a Glu-His-Fe triad in DHP A. From a comprehensive multiple-sequence alignment of amino acids (see the Supporting Information of ref 6), the M86 residue in DHP A has moderate sequence identity with other globins. On the basis of its proximity to H89, M86 was selected as a target amino acid for site-directed mutagenesis so that negatively charged amino acid residues could be replaced to possibly give rise to a charge relay. In this report, we discuss the X-ray crystal structures of mutants of residue M86 in DHP A, one of which folded in a conformation that resembles the charge relay found in peroxidases. The functional consequences of the creation of an Asp-His-Fe charge relay in a 3/3 globin were also examined using biochemical assays. Because the globin dehaloperoxidase has the highest reported peroxidase activity for the oxidation of phenolic substrates, the effects of a charge relay on the catalytic rate, redox potential, and ligand stabilization (trans effect) are crucial aspects of reactivity in globins, specifically, that lead to an improved understanding of peroxidase activity in heme enzymes, in general. The properties of the charge relay were studied systematically using X-ray crystallography, stopped-flow UV−vis spectroscopy, resonance Raman spectroscopy, spectroelectrochemistry, and ^{13}C nuclear magnetic resonance (NMR) of a heme Fe-bound, ^{13}C- and ^{15}N-labeled cyanide probe, with comparisons to density functional theory (DFT) calculations and molecular dynamics (MD) simulations

EXPERIMENTAL PROCEDURES

Materials. 2,4,6-Trichlorophenol (TCP, 98%), *N,N,N′,N′*-tetramethyl-*p*-phenylenediamine (TMPD, 95%), potassium ferricyanide {$[Fe(CN)_6]^{3+}$, >99%}, phenazine methosulfate (PhMS, 90%), hexaammineruthenium(III) chloride {$[Ru(NH_3)_6]^{3+}$, 98%}, methyl viologen (MV^{2+}, 98%), lysozyme, DNase, RNase, horse heart myoglobin (HHMb), horseradish peroxidase (HRP) type I, and all buffer salts (≥98% pure) were purchased from Sigma. Tris(ethylenediamine)ruthenium(II) tetrachlorozincate {$[Ru(en)_3]^{2+}$} was synthesized as previously described.[31,32] All other chemicals, unless specified, were purchased from Fisher Scientific.

Plasmid Preparation, Protein Expression, and Purification of Dehaloperoxidase-Hemoglobin A, M86D, M86E, and M86A. The pET-DHP4R plasmid[4] was used to produce DHP A, which has an N-terminal six-His tag. This plasmid was also used as the template DNA for the site-directed mutagenesis experiments. The oligonucleotide primers for mutagenesis for preparing the M86A mutant were as follows: 5′-CCAACACACTCGTCCAGGCGAAACAGCATTCCAGCC-3′ and 3′-GGTTGTGTGAGCAGGTCCGCTTTGTCGTAAGGTCGG-5′. Primers used to prepare the M86D mutant were as follows: 5′-CGCCAACACACTCGTCCAGGATAAACAGCATTCCAGCCTGA-3′ and 3′-GCGGTTGTGTGAGCAGGTCCTATTTGTCGTAAGGTCGGACT-5′. The primers used to prepare the M86E mutant were as follows: 5′-CCAACACACTCGTCCAGGAGAAACAGCATTCCAGCC-3′ and 3′-GGTTGTGTGAGCAGGTCCTCTTTGTCGTAAGGTCGG-5′. To crystallize the protein, the six-His tag needed to be removed and separate constructs were prepared. The histidine tag was removed from the 5′-end of the DNA sequences encoding the genes of M86D and M86E by using the QuikChange II XL site-directed mutagenesis kit with the following primers that were used in a previous study of the DHP B isoenzyme:[33] 5′-AGGAGATATACCATGGGGTTTAAACAAGAT-3′ (sense) and 5′-ATCTTGTTTAAACCCCATGGTATATCTCCT-3′ (antisense). The QuikChange II XL site-directed mutagenesis kit was used under the following three-step thermal cycling settings: first step (95 °C for 1 min), one cycle; second step [melt (95 °C for 50 s), anneal (60 °C for 50 s), and extension (68 °C for 6 min)], 18 cycles; third step (68 °C for 7 min), one cycle. The mutant Dpn I-treated DNA was transformed into XL-10 Gold ultracompetent *Escherichia coli* cells (from the mutagenesis kit) in Luria-Bertani (LB) medium. The transformed cells were grown to colonies on LB-ampicillin agar plates. The Qiaprep Spin Miniprep kit (Qiagen) was used to purify the mutated plasmid DNA, and the DNA sequence was verified by sequencing performed at Genewiz, Inc. (South Plainfield, NJ).

Each purified mutant DHP A plasmid was transformed into *E. coli* strain BL21-Gold(DE3) (Stratagene), and protein expression followed the procedure used for DHP A.[4] Briefly, purified six-His-tagged DHP A was first harvested from a 50 g BL21-Gold(DE3) cell pellet that was frozen at −80 °C. The cell pellet was resuspended in 100 mL of a cell lysis buffer [50 mM KPB (pH 8.0), 300 mM KCl, and 10 mM imidazole] at room temperature. Lyophilized lysozyme was added to the cell suspension to lyse the cells followed by sonication for 30 min at 4 °C. DNase and RNase were added to the cell lysate to lower the viscosity, and the cell lysate was centrifuged at 15000 rpm for 30 min. The supernatant, which contained the His-tagged DHP A enzyme, was loaded onto a nickel-immobilized metal affinity chromatography (Ni^{2+}-IMAC, Qiagen) column [1.5 cm (inside diameter) × 5 cm (length)]. Lysis buffer was used as a mobile phase to elute off proteins not having an affinity for the IMAC column. DHP A was subsequently eluted with 50 mM KPB (pH 8.0) containing 300 mM KCl and 250 mM imidazole. The DHP A sample was oxidized by the addition of $[Fe(CN)_6]^{3+}$ to the pooled DHP A fractions followed by dialysis (6−8 kDa molecular mass cutoff) against 10 mM KPB (pH 7.0) at 4 °C to remove ferri/ferrocyanide and imidazole. The dialysate was centrifuged at 12000 rpm for 30 min, and the supernatant that contained the DHP A sample was collected and loaded onto a CM-52 column [3.0 cm (inside diameter) × 6 cm (bed height)] pre-equilibrated with 10 mM KPB (pH 7.0) at 4 °C. Yellow impurity fractions eluted when the same 10 mM KPB buffer was passed through the column. The DHP A sample was then eluted using 38 mM KPB (pH 7.0). Pooled DHP A fractions were buffer exchanged into 10 mM KPB (pH 7.0) and concentrated to ca. 15 mL using an Amicon concentrator cell equipped with a YM-10 membrane (10 kDa molecular mass cutoff) (Millipore). DHP A was loaded onto a second identical CM-52 column and eluted with 18 mM KPB (pH 7.0). The leading edge of the band was discarded.

Purification of M86A was performed in the same manner as that of DHP A except for the use of only one CM-52 column [1.5 cm (inside diameter) × 8 cm (bed height); mobile phase of 18 mM KPB (pH 7.0)]. M86D and M86E were both purified in the same manner as DHP A except that 5 mM KPB (pH 7.0) was used for dialysis, column equilibration, and the first-column mobile phase.

The non-His-tagged DHP A M86D and M86E mutant proteins were transformed in *E. coli* Rosetta(DE3)pLysS cells (Stratagene), overexpressed, and purified by the procedures established for the purification of non-His-tagged DHP A.[34] Each purified protein already had the heme iron in the +3 oxidation state, judged by the Soret maximum at 413 nm, and no further oxidation with potassium ferricyanide was deemed necessary.

Purification of Horse Heart Myoglobin (HHMb) and Horseradish Peroxidase (HRP). The purification of HHMb and HRP type I followed previously published protocols[35,36] with minor modifications (see the Supporting Information).

Crystallization, Structure Determination, and Refinement. The purified non-His-tagged DHP A M86E and M86D mutants were each buffer exchanged into a 20 mM sodium cacodylate buffer (pH 6.5) followed by concentration to 8.0 mg/mL. Crystallization drops were set up by mixing the protein solution with an equal volume of precipitant solution and equilibrated against 600 μL of precipitant solution. This precipitant solution consisted of 0.2 M ammonium sulfate and PEG 4000 ranging from 30−36% (w/v). All experiments were conducted at 4 °C using the hanging drop vapor diffusion method. Each protein crystallized in the presence of 20 mM KCN, and the crystals appeared after 3 days; on the other hand, no crystals appeared in the presence of KF or in the absence of any added ligands. Crystallization of M86D-CN required a PEG 4000 concentration slightly higher than the percentage range used for M86E-CN. The best diffraction quality M86E-CN crystals grew from 0.2 M ammonium sulfate and 32% (w/v) PEG 4000. The crystals were allowed to grow for 7 days and were harvested into the mother liquor that was supplemented with 15% (w/v) PEG 400 as a cryoprotectant, and the crystals were flash-cooled in liquid nitrogen for data collection.

X-ray diffraction data for M86D-CN and M86E-CN crystals were collected at 100 K using a Rigaku RUH3R copper rotating anode generator (λ = 1.5418 Å) equipped with Osmics optics and a Mar345 image plate detector. The data sets were collected from a single crystal at a crystal−detector distance of 120 mm, using a 1° oscillation range and an exposure time of 5 min per image.

The diffraction data were indexed, integrated, and scaled using the HKL-2000 suite.[37] The crystals of M86D and M86E belong to space group $P2_12_12_1$, just like the crystals of DHP A (metaquo) (PDB entry 2QFK). The unit cell dimensions of M86D-CN are as follows: a = 60.37 Å, b = 67.50 Å, and c = 68.04 Å. The unit cell dimensions of M86E-CN are as follows: a = 58.56 Å, b = 67.42 Å, and c = 67.50 Å. Both sets are very close to the unit cell dimensions of the DHP A (metaquo) crystals.[34] The crystals diffracted at resolutions of 2.21 and 1.72 Å for M86D and M86E, respectively.

The structures of these two mutants were determined by molecular replacement with Phaser[38] using the metaquo structure of DHP A (PDB entry 2QFK)[34] as a search model. Cycles of refinement and map calculations were conducted with refmac5 from the CCP4 suite of programs,[39] iterated with model building using Coot.[40] The final model of M86E-CN was refined to an R factor of 18.4% (R_{free} = 24.3%) and contained two protein molecules with 94.8% of the residues in the most favored regions of the Ramachandran plot, with the remaining 5.2% in the additional allowed regions. M86D-CN was refined to an R factor of 23.0% (R_{free} = 29.3%) and contained two protein molecules with 95.2% of the residues in the most favored regions of the Ramachandran plot, with the remaining 4.8% in the additional allowed regions. The data collection and refinement statistics are listed in Table 1.

Spectroelectrochemistry (SEC). SEC was conducted in an airtight UV−vis spectroelectrochemical cell that utilized an optically transparent thin-layer electrode (OTTLE), namely, antimony−tin oxide (ATO) (Delta Technologies). This cell was similar to a previous design.[41] A nominal optical path length of 0.1 mm was realized using 0.1 mm thick Teflon-coated fiberglass tape (Small Parts, Inc.). The ATO electrode was cleaned before being used with 10 min successive sonications in a 1% (v/v) Contrex solution (Decon Laboratories, Inc.), 95% ethanol, and twice in deionized water.[22] The SEC cell was stored in a nitrogen-filled glovebox (Vacuum Atmospheres Co.) maintained at a sub-parts per million O_2 level for at least 8 h prior to experimentation. UV−vis spectra were recorded with a Hewlett-Packard 8453 spectrophotometer while potentials were controlled with a model 273A Princeton Applied Research potentiostat. The SEC cell made use of a Ag/AgCl (saturated KCl) reference electrode (Microelectrodes, Inc.) and a platinum wire auxiliary electrode (Alfa Aesar). All potentials reported are referenced to the standard hydrogen electrode (SHE). The electron transfer (ET) mediators TMPD and $[Ru(en)_3]^{2+}$ were used for DHP A and M86A to facilitate the transfer of electrons between the enzyme and the electrode, whereas $[Ru(Cl)_6]^{3+}$ was used as the mediator for M86E and M86D. The enzyme:mediator(s) ratio was 2:1. The concentration of ferric enzyme (DHP A or mutants) was in the range of 100−200 μM. Soret molar absorptivity values used to calculate concentrations were determined by the pyridine hemochrome assay.[42] Such values were recorded for the protein in 100 mM KPB (pH 7.0). The ε_{407} for DHP A is 116.4 mM^{-1} cm^{-1}.[42] The ε_{412} for M86E is 126.6 mM^{-1} cm^{-1}. The ε_{413} for M86D is 127.0 mM^{-1} cm^{-1}.

Table 1. X-ray Diffraction Data Collection and Refinement Statistics

	DHP A M86E-CN adduct	DHP A M86D-CN adduct
Data Collection		
space group	$P2_12_12_1$	$P2_12_12_1$
cell dimensions		
a, b, c (Å)	58.56, 67.42, 67.50	60.37, 67.50, 68.04
α, β, γ (deg)	90, 90, 90	90, 90, 90
temperature (K)	100	100
wavelength (Å)	1.54	1.54
resolution (Å)	1.72	2.21
R_{merge}[a] (%)	10.3 (77.3)[b]	13.8 (65.9)[b]
$I/\sigma(I)$	18.4 (2.5)[b]	5.8 (2.9)[b]
completeness (%)	99.9 (100.0)[b]	94.7 (97.7)[b]
redundancy	6.3 (6.2)[b]	7.0 (7.4)[b]
Refinement		
no. of reflections	27739 (2003)[b]	13557 (702)[b]
R_{work}[c] (%)	18.4	23.0
R_{free}[d] (%)	24.3	29.3
no. of atoms		
protein	2989	2632
water	322	199
rmsd[e] from ideal geometry		
bond lengths (Å)	0.01	0.01
bond angles (deg)	1.17	1.17
Ramachandran plot[f]		
most favored (%)	94.8	95.2
allowed (%)	5.2	4.8

[a] $R_{merge} = \sum_h\sum_i[|I_i(h) - \langle I(h)\rangle|/\sum_h\sum_i I(h)] \times 100\%$, where $I_i(h)$ is the ith measurement and $\langle I(h)\rangle$ is the weighted mean of all measurements of $I(h)$. [b] Values in parentheses are for the highest-resolution shell. [c] $R_{work} = \sum|F_O - F_C|/\sum F_O \times 100\%$, where F_O and F_C are the observed and calculated structure factors, respectively. [d] R_{free} is the R factor for the subset (5%) of reflections selected before and not included in the refinement. [e] Root-mean-square deviation. [f] Calculated using PROCHECK.[70]

The ε_{410} for M86A is 116.5 mM^{-1} cm^{-1}. The ε_{409} for HHMb is 185.0 mM^{-1} cm^{-1}. The ε_{403} for HRP type I is 102.0 mM^{-1} cm^{-1}.[35]

NMR Sample Preparation. The heme protein samples used for NMR experimentation were buffer exchanged and concentrated to ~600 μL in 100 mM KPB (pH 7.0) (D_2O solvent) using an Amicon Ultra-4, 10 kDa molecular mass cutoff filter (Millipore). To each ferric heme protein sample, 30 μL of 1.0 M isotope-labeled potassium cyanide ($K^{13}C^{15}N$, Cambridge Isotope Laboratories) was added to form the ferric-cyano adduct. Samples were run in a 5 mm NMR tube; TMS was used as an internal standard, and all spectra were recorded at 295 K.

^{1}H and ^{13}C Paramagnetic NMR Spectroscopy. Pulsed field NMR experiments were performed on a Bruker AVANCE 500 MHz spectrometer (1996) with an Oxford narrow bore magnet (1989), Linux host workstation (RedHat), and TOPSPIN version 1.3 (Bruker). The instrument was equipped with three frequency channels with waveform memory, an amplitude shaping unit with a three-channel gradient control unit (GRASP III), and a 5 mm inside diameter 1H/BB (^{109}Ag−^{31}P) triple-axis gradient probe (ID500-5EB, Nalorac Cryogenic Corp.) and a single-frequency ^{13}C probe (General

Electric) adapted for use with the Bruker upper stack. The latter probe was used for all ^{13}C NMR measurements.

The operational frequencies for the ^{1}H and ^{13}C nuclei were 500.128 and 125.757 MHz, respectively. One-dimensional (1D) ^{1}H NMR spectra were obtained by using a spectral width of 32 kHz, 32768 (32K) data points, 256 transients, and a water presaturation pulse sequence with a power of 55 dB. The pulse repetition time totaled 2.5 s (2 s relaxation time and 500 ms acquisition time). A pulse of 10.5 μs was used to acquire the ^{1}H spectra. 1D ^{13}C NMR spectra were obtained in analog mode using a spectral width of 200 kHz; the zgdc pulse sequence was used with a waltz16 decoupling modulation and 8192 (8K) data points. The pulse repetition time totaled 95 ms (75 ms relaxation time and 20 ms acquisition time), and an 8 μs pulse was applied to acquire the ^{13}C spectra. To flatten the baseline, the DE prescan delay value was increased to 20 μs. Because the typical heme protein sample had a concentration of 1.5 mM, 1 million transients were needed to obtain a suitable signal:noise ratio.

The processing parameters used in TOPSPIN version 1.3 were 2048 data points, 20 raw data points, backward real linear prediction, a linear prediction coefficient of 32, and an exponential function with 1000 Hz line broadening. To proceed with the linear prediction method, the data were converted with digital filters using the "convdta" command.

UV−Vis Spectrophotometric Steady State Activity Assays. Assays were conducted in a 1.0 cm path length quartz microcuvette in a Cary 50 UV−vis spectrophotometer having a thermostated cell holder at 25 °C. Prior to any assay, a slight excess of potassium ferricyanide was added to a heme protein sample so that it would be in the ferric oxidation state. The sample was purified from the ferri/ferrocyanide species by using a PD-10 desalting column prepacked with Sephadex G-25 medium (GE Healthcare). The protein was subsequently concentrated with an Amicon Ultra-4 centrifugal filter (10 kDa molecular mass cutoff). Concentrations were determined using molar absorptivity values determined by the pyridine hemochrome assay (see above).[42] Apparent K_M and k_{cat} values were calculated from three trials of initial rate (ν_o) measurements at each H_2O_2 concentration at a fixed concentration of 2,4,6-trichlorophenol substrate. GraFit (Erithacus Software) was used to fit the experimental data to the Michaelis−Menten model. Enzymatic activity was assayed with respect to the decrease in TCP concentration (λ_{max} = 312 nm). Each reaction mixture had a total volume of 1.0 mL in which the heme protein concentration was fixed, the TCP concentration was 150 μM, and various H_2O_2 concentrations that ranged from 10 to 750 μM were present in 100 mM KPB (pH 7.0).

Stopped-Flow Kinetics. Stopped-flow kinetics experiments were conducted using a Bio-Logic SFM-400 triple-mixing stopped-flow instrument linked with a rapid scanning diode array UV−vis spectrophotometer. The temperature was maintained at 20 °C with a circulating water bath. Data were collected (900 scans total) over a three-time domain regime (2.5, 25, and 250 ms; 300 scans each) using the Bio Kinet32 software package (Bio-Logic). In a typical single-mixing experiment, the ferric DHP A mutant (having a final concentration of 10 μM) was mixed with 2.5−25 equiv of H_2O_2. All data were evaluated using the Specfit Global Analysis System software package (Spectrum Software Associates) and fit to exponential functions as either one-step, two-species or two-step, three-species irreversible mechanisms, where applicable. Kinetics data were baseline corrected using the Specfit autozero function.

Resonance Raman Spectroscopy. Resonance Raman spectra were recorded by Soret band excitation using a Coherent Mira 900 titanium sapphire (Ti:sapphire) laser. The Ti:sapphire laser was pumped using a Coherent Verdi 10 frequency-doubled diode-pumped Nd:vanadate laser generating 10 W at 532 nm. The beam generated from the Ti:sapphire laser can be tuned through approximately 700−1000 nm and was passed through a Coherent 5-050 doubler to generate a normal working range of 400−430 nm for Soret band excitation. The beam was collimated and cylindrically focused to a vertical line of ∼0.5 mm on the sample. Scattered light was collected with a Spex 1877 triple spectrometer (2400 grooves/mm final stage grating) equipped with an ISA SPEX liquid nitrogen-cooled CCD at ∼1.7 cm^{-1} resolution. Computer acquisition of the data was accomplished with SpectraMax version 2.0. The spectra were calibrated using known peaks from indene, toluene, and carbon tetrachloride standards.

Molecular Dynamics Simulations of the M86D and M86E Mutants. Molecular dynamics (MD) simulations were conducted using NAMD.[43] The A-chain structure in PDB entry 2QFK was used to create a model for a monomer of DHP A.[44] Mutations in the M86 position were created using the mutate residue function in VMD.[45] The ε-tautomer of H55 and the δ-tautomer of H89 were used in the simulation. The default setting in VMD is the δ-tautomer, and this required editing of the PDB file to install the proper template. The δ- and ε-tautomers are given the names HSD and HSE, respectively, in the PDB file. Periodic boundary conditions were used with a padding of 10 Å in each dimension to give 50.5 Å × 57.2 Å × 60.3 Å boxes for both M86D and M86E structures. There were 4488 water molecules included; the effective ionic strength was 0.5, corresponding to 23 Na^+ ions and 21 Cl^- ions, and the cutoff distance was 12 Å, with a 2 Å switching distance.

Density Functional Theory Calculations. The model system used in this study consisted of two 4-methylimidazole (4-MeIm) ligands bound to a heme (H) with truncated propionate groups. The optimized ground state geometries and potential energy surfaces of 4-MeIm-FeH-4-MeIm were obtained using the GBE functional[46,47] as implemented in DMol3.[48,49] All calculations were conducted on the ARC cluster at North Carolina State University. Geometry optimizations were conducted without constraints until the energy difference was less than 10^{-6} a.u. on subsequent iterations (Supporting Information). Numerically tabulated basis sets of double-ζ plus extra polarization (DNPP) quality were employed (as described in the Supporting Information). The potential energy surfaces were calculated for both Fermi (canonical ensemble)[50] and Thermal (grand canonical ensemble) treatments of the density functional.[51] The grand canonical option always converged to a lower overall energy. The grand canonical calculation was conducted at an electronic temperature (k_BT) of 0.02 eV. Once a calculation was complete, it was extrapolated to zero temperature by subtraction of the thermal electron occupation according to the grand canonical partition function.

RESULTS

The functional and structural consequences of installing an Asp-His-Fe triad in DHP A M86D have been explored by X-ray crystallography, electrochemistry, spectroscopy (NMR and resonance Raman), and kinetic assays that aimed to understand

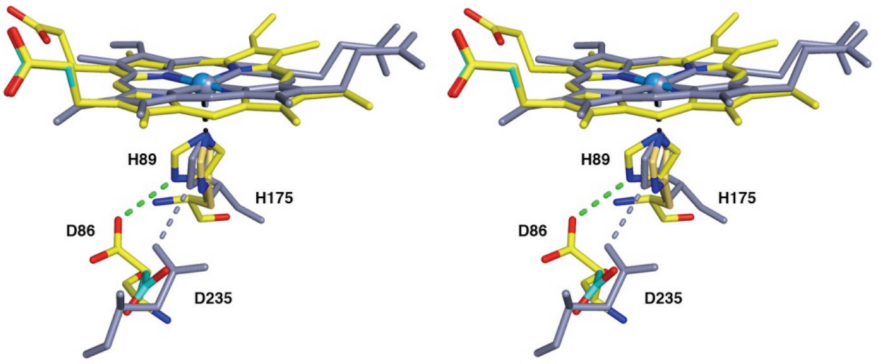

Figure 1. Structural comparison of the Asp-His-Fe triads observed in DHP A M86D and wild-type C*c*P. Superposition of chain B of M86D (PDB entry 3MYN) (yellow for C, red for O, blue for N, Fe^{3+} as a blue sphere, hydrogen bonds as green dashed lines; carbon atoms are colored gold and cyan for equal- and lower-occupancy conformers, respectively) and wild-type C*c*P (PDB entry 1CCA)[14] (all atoms and interactions are colored gray). The D86−H89 hydrogen bond in M86D has an O−N separation of 2.9 Å, and the D235−H175 hydrogen bond in C*c*P has an O−N separation of 3.0 Å. The superposition is based on the alignment of the heme Fe and the proximal histidine N_ε atom between the two structures.

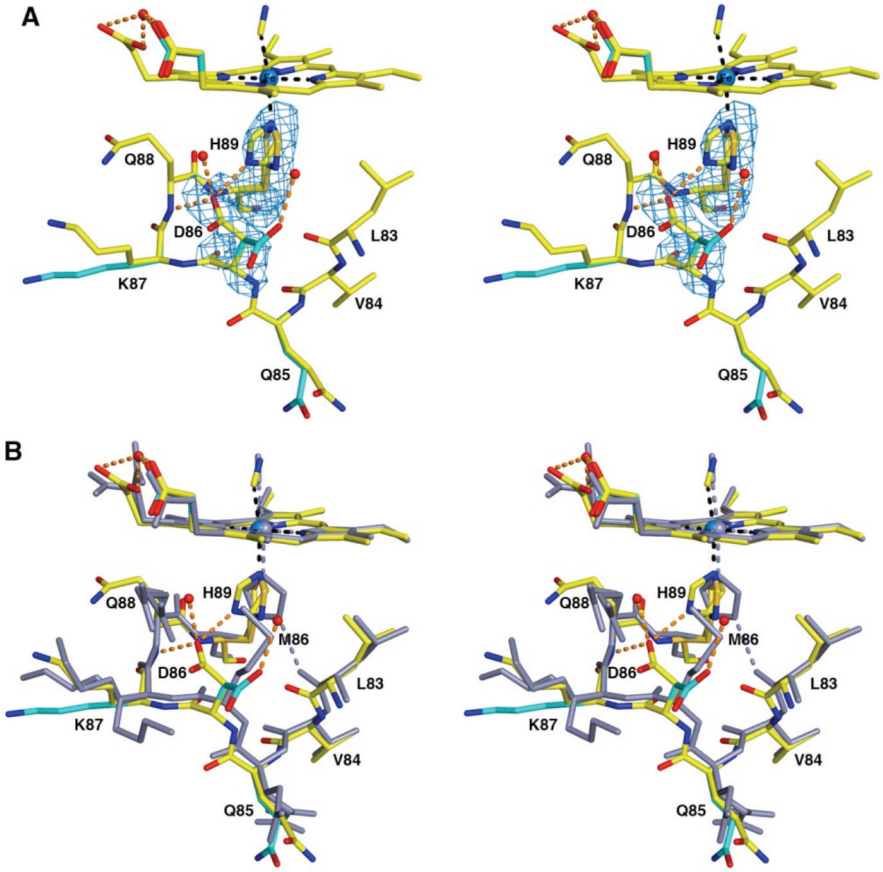

Figure 2. DHP A M86D-CN complex at pH 6.5. (A) Simulated annealing omit maps (blue) are contoured at 2.5σ for residues D86 and H89. H89 is found rotated substantially from the conformation in the wild-type structure and forms a hydrogen bond with D86 (O−N separation is 2.9 Å). Atoms are represented by the following color scheme: yellow for C, red for O, blue for N, Fe^{3+} as a marine blue sphere, solvent as red spheres; carbon atoms are colored cyan and gold in residue side chains with lower- and equal-occupancy conformers, respectively. Iron coordination interactions are represented by black dashed lines, and hydrogen bonds are represented as orange dashed lines. (B) Superposition of chain B of M86D-CN (same coloring scheme as in panel A) and chain A of DHP A-CN [X-ray data from a rotating anode source (unpublished results); all atoms colored gray].

the redox, electrostatic, and catalytic consequences. Moreover, we have compared the three mutations in DHP A (M86A, M86D, and M86E) to understand the systematic effect of altering the charge density at site M86. The comparison of the enzymatic rates of these three mutants shows a trend that is opposite to what one might expect on the basis of the installation of the charge relay. M86D has the smallest rate despite the Asp-His-Fe charge relay. This is a crucial measurement because it suggests that there is a competing effect, which we consider to be increased six-coordination by either water or H55. The experimental data were augmented by dynamic and energetic information obtained from MD

dx.doi.org/10.1021/bi201368u | *Biochemistry* 2011, 50, 9664−9680

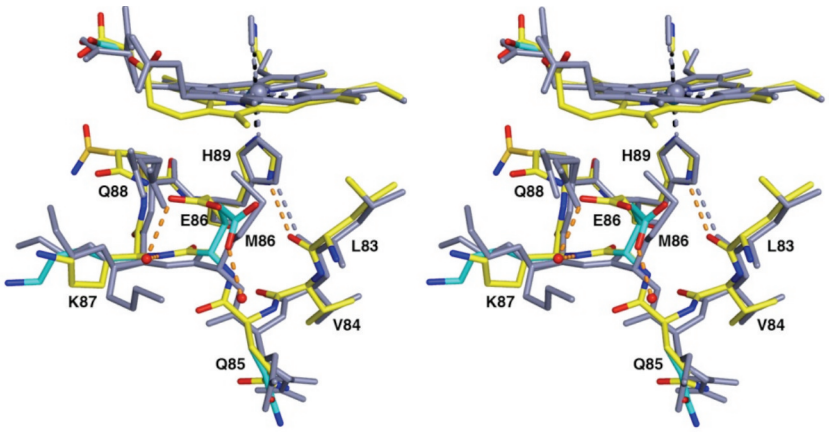

Figure 3. DHP A M86E-CN complex at pH 6.5. Superposition of chain B of M86E-CN (yellow for C, red for O, blue for N, Fe^{3+} as a marine blue sphere, solvent as red spheres, iron coordination as black dashed lines, hydrogen bonds as orange dashed lines; carbon atoms are colored cyan and gold in residue side chains with lower- and equal-occupancy conformers, respectively) and chain A of DHP A-CN [X-ray data from a rotating anode source (unpublished results); all atoms colored gray]. E86 is solvent-exposed and does not interact with H89, and H89 remains hydrogen bonded with the backbone carbonyl of L83.

simulations and DFT calculations that aimed to understand the potential effects of M86 mutations on the heme Fe binding affinity for the distal histidine.

Crystal Structure of DHP A M86D-CN. The structure of M86D-CN has an overall fold identical to that of DHP A-CN, determined using a data set collected in house with a root-mean-square deviation (rmsd) of 0.52 Å for 137 C_α atoms.[52] Figure 1 shows a comparison of the proximity of the proximal histidine to Asp-86 in DHP A(M86D) and to the Asp-235 residue in C*c*P. The similarity of the distances in these two structures suggests that such an active catalytic triad has been installed in DHP A. A simulated annealing omit map (sa-omit map) of residues H89 and D86 (Figure 2A) reveals the formation of a D86-H89-Fe triad located in the proximal region of the enzyme. The D86 and H89 residues are observed in two conformations in chain A and chain B of the asymmetric unit with occupancies ranging from 0.4 to 0.6 from each conformer. The triad revealed by the M86D-CN variant has the imidazole ring of H89 rotated more toward D86 (a superposition of DHP A-CN and the M86D-CN structures is shown in Figure 2B). The separation between the L83 carbonyl oxygen and the H89 N_δ atom is 3.6 Å in both chains (for the closer H89 conformer). This hydrogen bond observed in wild-type DHP A is considerably weakened in favor of an Asp−His interaction, in which the H89 N_δ atom and the closer aspartate carboxylate oxygens of D86 have separations of 3.0 and 2.9 Å in chains A and B, respectively. The L83 carbonyl is farther (4.3 Å in chain A and 4.5 Å in chain B) from the relevant H89 N_δ atom. With respect to DHP A-CN, the Q88 side chain is moved away from the formed D86-H89-Fe triad as shown in Figure 2B.

Crystal Structure of DHP A M86E-CN. The structure for the cyanide-bound form of M86E (M86E-CN) has an overall fold similar to that of DHP A-CN with an rmsd of 0.53 Å for 137 C_α atoms. The proximal region of this structure that has relevant structural changes because of the mutation is shown in Figure 3. Residue E86 is observed in two conformations that are solvent-exposed, and one of the conformers has interactions with the side chain of Q88 as shown in Figure 4. Figure 4 shows a comparison of the position of E86 to that of D86. The M86E mutation does not give rise to a Glu-His-Fe triad as evidenced by a shortest carboxylate oxygen−H89 N_δ separation of 3.5 Å (chain A) or 5.5 Å (chain B).

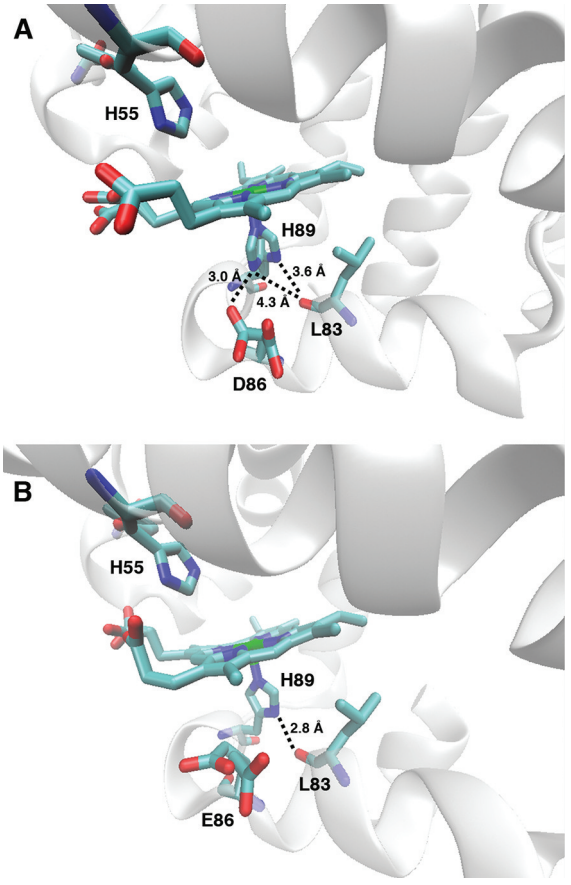

Figure 4. Structural comparison of the DHP A proximal region mutants (A) M86D-CN (chain A) and (B) M86E-CN (chain B). Relevant hydrogen bonding distances are shown. For the sake of clarity, only the shortest distance between (D86)O_δ and (H89)N_δ is shown in panel B and the heme Fe cyanide ligand was omitted from both panels.

UV−Vis Spectroelectrochemistry. The three mutants, M86A, M86E, and M86D, follow a trend of decreasing reduction potential (M86D < M86E < M86A ≈ wild type) consistent with the relative importance of the charge relay. The stronger the charge relay, the greater the stabilization of the

dx.doi.org/10.1021/bi201368u | *Biochemistry* 2011, 50, 9664−9680

Table 2. Michaelis–Menten Constants from Enzymatic Activity, Oxidation–Reduction Potentials, ^{13}C Chemical Shifts (Fe-CN), and O–O Bond Cleavage Rate Constants of H_2O_2 for DHP A and the M86 Mutants

	DHP A	M86A	M86E	M86D
Michaelis–Menten constant,[a] K_M(μM)	23 ± 1.2	50 ± 5.9	60 ± 3.8	200 ± 29
oxidation–reduction potential,[b] $E^{\circ\prime}$ (mV), vs SHE	202 ± 6[c]	200 ± 6	112 ± 11	76 ± 5
^{13}C chemical shift (Fe-CN),[d] $\Delta\delta_{para}$ (ppm)	0	−15	59	131
ES formation rate constant,[e] k_{obs} (M^{-1} s^{-1}/10^4)	3.56 ± 0.02[f]	0.88 ± 0.01	0.36 ± ~0.01	–

[a]Reactants were 150 μM TCP (fixed concentration) and H_2O_2 (various concentrations ranging from 10 to 750 μM). [b]Oxidation–reduction potentials for the Fe(III)/Fe(II) couple under anaerobic conditions. [c]From ref 63. [d]^{13}C- and ^{15}N-labeled cyanide bound to Fe(III) was used as the probe. Resonance position with respect to DHP A (−4211 ppm). [e]Observed rate constant for formation of compound ES. [f]From ref 11.

ferric form. The anaerobic Fe(III)/Fe(II) formal reduction potentials at pH 7.0 and 25 °C for the DHP A Met-86 mutants are listed in Table 2. The M86A mutant has a reduction potential of 200 ± 6 mV versus SHE, which is similar to that of wild-type DHP A ($E^{\circ\prime}$ = 202 ± 6 mV). The M86E and M86D mutants, however, had significantly lower values of 112 ± 11 and 76 ± 5 mV, respectively. Figure 5A displays representative

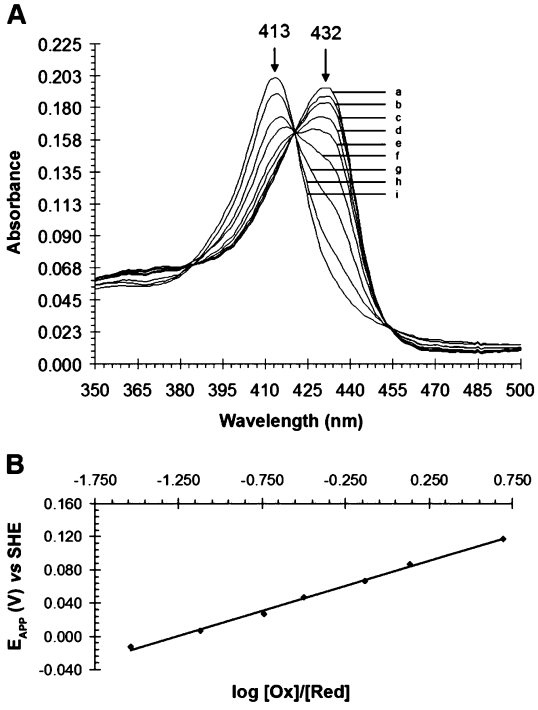

Figure 5. UV–vis thin-layer spectroelectrochemistry of M86D. (A) Spectra are shown for M86D in 100 mM potassium phosphate (pH 7.0) at 25 °C with a $[Ru(NH_3)_6]^{3+}$ mediator, at applied potentials (E_{APP} vs SHE) of (a) −0.303, (b) −0.013, (c) 0.007, (d) 0.027, (e) 0.047, (f) 0.067, (g) 0.087, (h) 0.117, and (i) 0.197 V. (B) Nernst plot of the same data.

SEC spectra obtained at various applied potentials (E_{APP}) for M86D. These spectra can be used to obtain the equilibrium concentrations of the oxidized (ferric, 413 nm) and reduced (deoxyferrous, 432 nm) forms of M86D. The resultant Nernst plot shown in Figure 5B has a slope of 59.9 mV, which corresponds to an n = 1 redox reaction.[53]

Paramagnetic ^{1}H and ^{13}C NMR Spectroscopy. The paramagnetic shift of ^{13}C- and ^{15}N-labeled cyanide parallels the redox potential (M86D < M86E < M86A ≈ wild type), which is consistent with the increased shielding provided by the trans effect as the charge relay increases in donation strength. ^{1}H and ^{13}C NMR spectra of the ^{13}C- and ^{15}N-labeled cyanide-bound ferric forms of DHP A, M86A, M86E, M86D, HHMb, and HRP type I were recorded at pH 7.0 and 25 °C. Panels A and B of Figure 6 show the ^{13}C NMR spectra that were obtained. Our

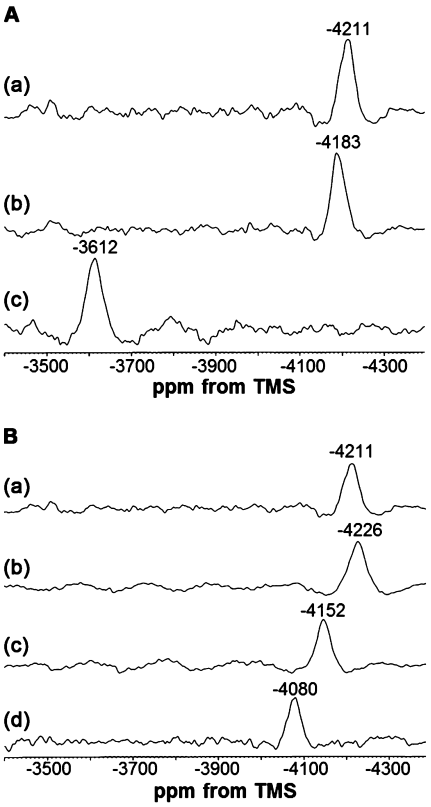

Figure 6. ^{13}C paramagnetic NMR spectra of various heme proteins. Spectra are shown for ^{13}C^{15}N bound to the heme Fe of (A) heme proteins (a) DHP A, (b) HHMb, and (c) HRP type I and (B) comparison of (a) DHP A with (b) M86A, (c) M86E, and (d) M86D.

^{1}H NMR results (not shown) are in good agreement with previously published spectra for the metcyano forms of HRP at pH 7.6,[54] SWMb at pH 8.6,[55] and DHP A at pH 7.0.[56] ^{13}C NMR spectra obtained for HHMb (−4183 ppm) and HRP type I (−3612 ppm), which served as controls, are also in good agreement with a previous report.[57] DHP A exhibits a ^{13}C NMR paramagnetic shift of −4211 ppm with respect to trimethylsilane (TMS). Downfield shifts (relative to the wild type) of 59 and 131 ppm were observed for Fe(III)-^{13}C^{15}N forms of M86E and M86D, respectively (Table 2), while a small upfield shift of 15 ppm was observed for the M86A mutant.

dx.doi.org/10.1021/bi201368u | Biochemistry 2011, 50, 9664–9680

Table 3. Steady State Enzymatic Assay of Various Proteins with 2,4,6-Trichlorophenol (TCP) and H_2O_2 at pH 7.0[a]

protein	k_{cat} (s^{-1})	K_M (μM)	wt activity (%)	k_{cat}/K_M (μM^{-1} s^{-1})
DHP A	0.61 ± 0.01	23 ± 1.2	100	0.027
M86D	1.3 ± 0.07	200 ± 29	213	0.0065
M86E	0.97 ± 0.02	60 ± 3.8	159	0.016
M86A	0.94 ± 0.03	50 ± 5.9	154	0.019
HHMb	0.065 ± 0.002	200 ± 22	10.7	0.00033
HRP type I	17.5 ± 1.9	30 ± 13	~2900	0.58

[a]See the text for experimental details. Indicated errors represent one standard deviation.

Steady State Activity. The catalytic efficiency of the charge relay mutants is opposite of the expected trend based on known peroxidase behavior (M86D < M86E ≈ M86A < wild type). The activities of DHP A, the M86 mutants, HHMb, and HRP type I were assayed at pH 7.0 and 25 °C (Table 3). HHMb was found to have ~10% of the wild-type DHP A activity for conversion of 2,4,6-trichlorophenolate (TCP) to 2,6-dichloroquinone (DCQ), compared to ~2900% for HRP type I (based on the k_{cat} parameter). These results parallel the findings of a previous report,[4] which found DHP A to be ~1 order of magnitude more active than Mb and ~1 order of magnitude less active than HRP when using TBP as a substrate at pH 5.0. Table 3 shows that all three M86 mutants were more active than wild-type DHP A in the conversion of TCP: M86D (213%) > M86E (159%) ≈ M86A (154%). The K_M values, on the other hand, indicated weaker H_2O_2 binding in all three M86 mutants relative to that of the wild-type protein: M86D (200 μM) > M86E (60 μM) > M86A (50 μM) > DHP A (23 μM). The similarity of the K_M values for HHMb (200 μM) and M86D confirms that H_2O_2 reactivity is low in these two globins. Values obtained for the efficiency parameter (k_{cat}/K_M) reveal DHP A to be more reactive than all three M86 mutants, even though the turnover number is lower (Table 3).

Stopped-Flow Kinetics. The kinetic observations by stopped-flow UV−vis parallel the steady state measurements. The M86D mutant has the lowest activity despite the structural, electrochemistry, and NMR data, which are all consistent with the increased trans effect of the charge relay. Typical results obtained from the stopped-flow studies are shown in Figure 7 for M86E. When ferric DHP A M86E [UV−vis spectrum: 413 (Soret), 528, 563, 636 nm (Figure 7B, black trace)] was rapidly mixed (2 ms) with a 10-fold excess of H_2O_2, formation of a new intermediate whose spectral features [UV−vis spectrum: 419 (Soret), 546, 588 nm (Figure 7B, red trace)] closely resembled those of a ferryl-containing intermediate (e.g., Compound II or ES) was observed. On the basis of the previous identification of such reaction intermediates in wild-type DHP A, the ferryl intermediate here is assigned as Compound ES. Compound I, which is characterized by a major hypochromic shift in the Soret band,[58] was not observed on the time scale of these experiments. The experimental values of k_{obs} for ferryl formation varied linearly with H_2O_2 in the range of 2.5−25 molar equiv (data not shown). From this dependence, the bimolecular rate constant was determined to be (0.36 ± ~0.01) × 10^4 M^{-1} s^{-1} (Table 2). In the absence of a reducing substrate, Compound ES was found to be unstable and interconverted to a stable species [UV−vis spectrum: 413 (Soret), 539 nm (Figure 7B, blue trace)] that has been previously designated as Compound RH in wild-type DHP A.[11] The corresponding kinetic data for the M86A mutation are presented in Figure S1 of the Supporting Information.

For the M86A mutant, the results were qualitatively similar to those observed for the M86E mutant above. Briefly, a Compound ES intermediate [UV−vis: 419, 546, 588 nm; k_{obs} = (0.88 ± 0.01) × 10^4 M^{-1} s^{-1}] was also observed upon reaction of ferric DHP A M86A (UV−vis: 410, 526, 564, 636 nm) with a 10-fold excess of hydrogen peroxide (Supporting Information). The M86A Compound ES intermediate was also unstable and converted to Compound RH [UV−vis spectrum: 414 (Soret), 543, 579 nm] in the absence of an exogenously added substrate. Values of the observed rate constant (k_{obs}) for the formation of Compound ES are listed in Table 2 for DHP A, M86A, and M86E. Compound ES formation became significantly impaired as a result of the M86A and M86E mutations, as reflected by 4- and 10-fold decreases in k_{obs}, respectively.

By contrast to the other mutants studied, a k_{obs} value could not be determined for the M86D mutant because quantitative formation of the Fe(IV)-ferryl intermediate (as monitored by the Soret band shift) does not occur at a H_2O_2 level of ≤1000 equiv (results not shown). Although quantitative formation of the Fe(IV)-ferryl species could be achieved upon mixing M86D with 10000 equiv of H_2O_2 (Soret band red-shifted from 413 to 418 nm), the protein suffered rapid denaturation (Figure S2 of the Supporting Information).

Resonance Raman Spectroscopy. Resonance Raman spectroscopy was applied to the study of the ligation state of the heme iron to seek a possible explanation for the discrepancy between the structural and kinetic data. Resonance Raman spectra for the ferric form of M86D (pH 7.0) in the presence and absence of cyanide ion are shown in Figure 8A. The M86D-CN complex (M86D-CN) exhibits peaks that are characteristic of hexacoordinate low-spin (6cLS) modes, such as ν_3 (1505 cm^{-1}), ν_2 (1582 cm^{-1}), $\nu_{C=C}$ (1620 cm^{-1}), and ν_{10} (1638 cm^{-1}).[59,60] The DHP A-CN complex has previously been reported for the ν_3 (1502 cm^{-1}) and ν_2 (1582 cm^{-1}) modes, which are consistent with our results for this Fe(III)-cyano mutant.[61,62] The resonance Raman spectrum observed for M86D in the absence of cyanide ion is similar to the spectrum of M86D-CN except for the $\nu_{C=C}$ and ν_{10} modes, which overlap as one unresolved peak (1629 cm^{-1}) rather than being observed as two resolved peaks at 1620 cm^{-1} ($\nu_{C=C}$) and 1638 cm^{-1} (ν_{10}). This finding is reminiscent of the C*c*P H181G mutant at pH 7.0 that was assigned as the bis-histidyl complex.[60] Although cyanide-free and cyanide-bound M86D resonance Raman spectra are similar (Figure 8A), their UV−vis spectra are not (Figure S3 of the Supporting Information), which indicates that M86D is a 6cLS species and that cyanide is capable of displacing its sixth ligand. The UV−vis spectrum for M86D-CN is similar to that of DHP A-CN,[61,62] which reveals that cyanide is bound to the M86D mutant and that the sixth ligand in cyanide-free M86D is strong field and internal.

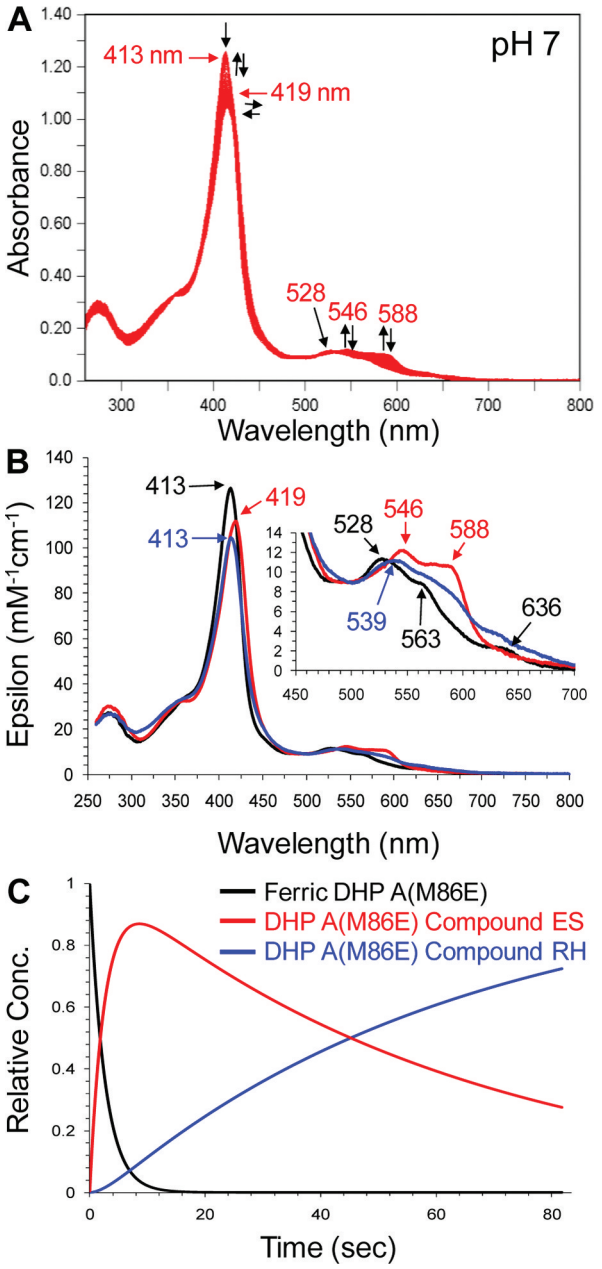

Figure 7. Single-mixing stopped-flow kinetics of the DHP A M86E mutant with hydrogen peroxide. (A) Single-mixing stopped-flow UV–vis spectroscopic monitoring of the reaction (900 scans, 85 s) between DHP A M86E (10 μM) and a 10-fold excess of H_2O_2 at pH 7.0 (see Experimental Procedures for details). (B) Calculated UV–vis spectra for resting (black), Compound ES (red), and the putative species Compound RH (blue) of DHP A M86E. The rapid-scanning data from panel A were compiled and fitted to a double-exponential reaction model using the Specfit global analysis program. (C) Relative concentration profile determined from the three-component fit used in panel B.

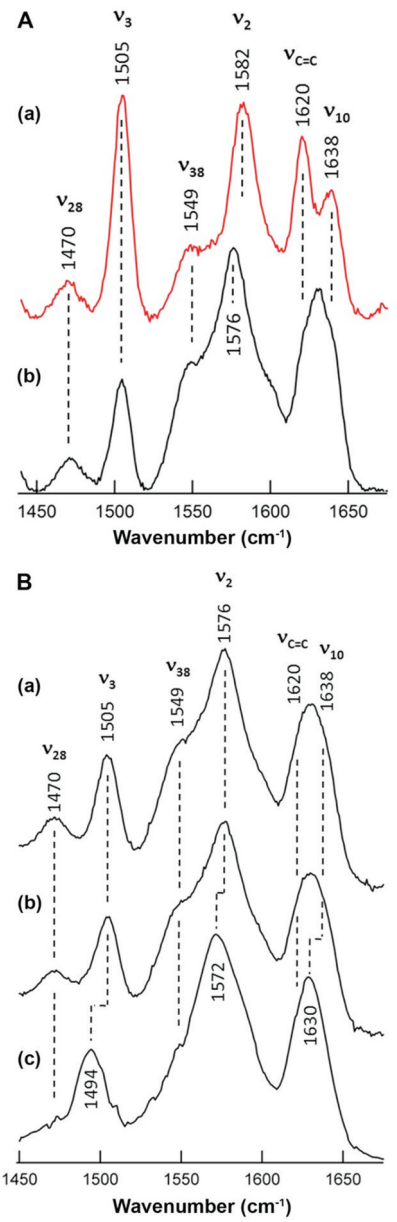

Figure 8. Resonance Raman spectra of M86D in the presence and absence of cyanide ion. (A) Ferric forms of (a) M86D-CN and (b) M86D at pH 7.0. (B) Ferric forms of M86D at (a) pH 7.0, (b) 6.0, and (c) 5.0.

The pH dependence of the sixth ligand in cyanide-free M86D can be seen in the resonance Raman spectra shown in Figure 8B. The pH 7.0 and 6.0 spectra are nearly identical and indicate a 6cLS heme with ν_3 at 1505 cm^{-1}, ν_2 at 1582 cm^{-1}, $\nu_{C=C}$ at 1620 cm^{-1}, and ν_{10} at 1638 cm^{-1}. These two spectra reflect the resonance Raman spectrum of M86D shown in Figure 8A, also at pH 7.0. At pH 5.0, however, the resonance Raman spectrum of M86D is indicative of a pentacoordinate high-spin (5cHS) heme with ν_3 at 1494 cm^{-1}, ν_2 at 1572 cm^{-1}, and ν_{10} at 1630 cm^{-1}. The energies of ν_2 and ν_{10} vary slightly from those of DHP A (1568 and 1632 cm^{-1}, respectively), but this can likely be attributed to the mutated proximal heme environment affecting the out-of-plane iron in the 5cHS species. Nevertheless, the change in the coordination and spin state of the heme iron is a phenomenon driven by pH and is not a response to on–off H_2O binding. This evidence further supports the possibility that M86D forms a bis-histidyl complex.

Density Functional Theory Calculations. DFT calculations were employed to study the possible electronic effects that lead to stabilization of a six-coordinate bis-histidine adduct suggested by the resonance Raman spectral data. The DFT calculations show that the Fe–N bond strength increases when polarization of the Fe–N bond increases. This trend can be

dx.doi.org/10.1021/bi201368u | *Biochemistry* 2011, 50, 9664–9680

Table 4. Calculated Fe−N_ε Bond Lengths, Mulliken Charges, and Binding Energies Based on the DFT Model for Bis(4-methylimidazole) Adducts in Various Charge States and Fe Oxidation States

			Mulliken charge		
4-Melm orientation	species	bond length (Å)	heme Fe	4-MeIm (N_ε)	binding energy (kcal/mol)
distal	ferric dianion	1.994	0.734	−0.290	−31.1
	ferric anion	1.917	0.741	−0.297	−40.8
	ferric	2.046	0.740	−0.257	−27.7
	ferrous	2.011	0.685	−0.246	−24.2
proximal	ferric dianion	1.982	0.734	−0.292	−31.1
	ferric anion	2.081	0.741	−0.262	−25.7
	ferric	2.046	0.740	−0.266	−27.7
	ferrous	2.012	0.685	−0.253	−24.2

quantitated using the Mulliken charge on the heme Fe and imidazole nitrogens. Table 4 shows that the greater the differential charge on the heme Fe and N_ε atom of the proximal or distal histidine, modeled as 4-methylimidazole (4-MeIm), the shorter the bond length. The ferrous heme model shows a difference compared to the ferric heme models, which follows the trend completely. The bond strength is also correlated with the Fe−N bond length (Figure 9). The ferrous neutral adduct has a bond length of ∼2.012 Å and the smallest bonding energy of ∼24.2 kcal/mol compared to those of the presented adducts. The ferric neutral adduct has an Fe−N bond length and energy of 2.046 Å and ∼27.7 kcal/mol, respectively. The symmetric dianion adduct has even shorter bond lengths (1.994 and 1.982 Å) and stronger Fe−4-MeIm bonds (∼31.1 kcal/mol). The trans effect is more complex for the asymmetric complexes, which are represented by the monoanion in our calculation. On the basis of the Mulliken charge, we can make one of the imidazoles more negative than the other. In this case, the negatively charged 4-MeIm has the strongest bond of any species in the comparison group with a bond length of 1.917 Å and a binding energy of 40.8 kcal/mol. However, the neutral histidine has a longer bond length, and its binding energy is relatively small compared to that of the dianion or even the ferric neutral species.

Molecular Dynamics Simulations. MD simulations show that the geometry for formation of a bis-histidine adduct is feasible in DHP A. While this may not be surprising given the tendency of heme proteins to form the hemichrome structure, it is still a verification that is important for the model proposed here based on the data. The details of hemichrome formation are poorly understood because a hemichrome is an intermediate in the unfolding and degradation of hemoglobins. The UV−vis and resonance Raman data provide corroborating evidence that there is ligation by the distal histidine. The purpose of the calculations was to determine whether this model is consistent with the geometry and electronic structure of the heme adducts that could form in the M86D mutant of DHP A. The charge sets used for ferric heme and imidazolate are reported in the Supporting Information. The DFT calculations reported above are a part of the process of deriving parameters for the force field to be used in NAMD, and these details are also discussed in the Supporting Information. Neutral imidazole does move close enough to the heme Fe and orients in a favorable position to potentially form a bond as shown in Figure S4 of the Supporting Information. However, Figure S4 shows that it does not adopt a true bonding conformation. Calculations were also conducted with the imidazolate charge set. In that case, the contact between the N_ε atom of the distal histidine and the iron is

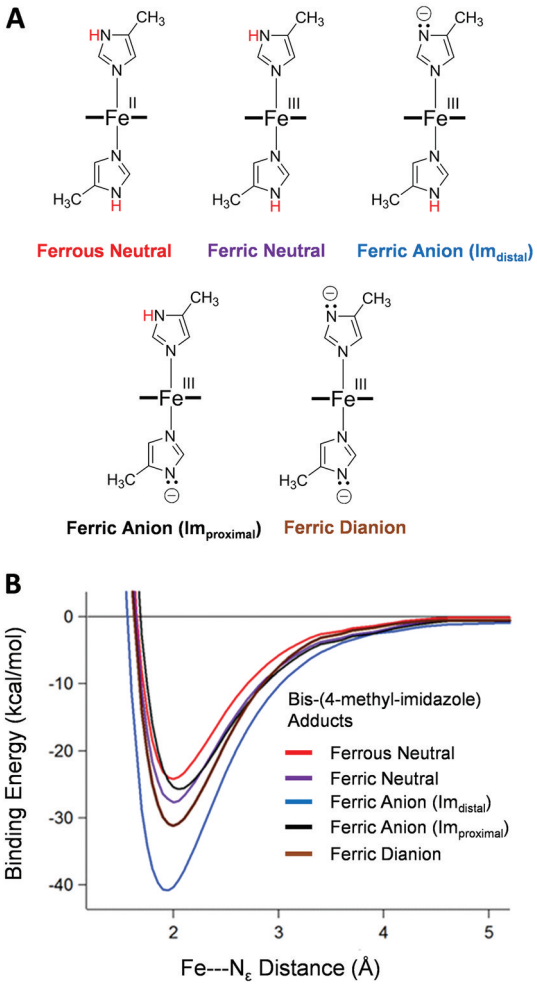

Figure 9. Potential energy surfaces along the Fe−N_ε bond for 4-methylimidazole binding to the heme Fe. (A) Bis(4-methylimidazole) adducts for various charged heme species. (B) Plot of Fe−N_ε binding energy as a function of Fe−N_ε bond distance: red for ferrous neutral, violet for ferric neutral, blue for ferric anion (Im_{distal}), black for ferric anion ($Im_{proximal}$), and brown for ferric dianion.

indicative of a bonded conformation. As Table 4 shows the DFT calculations, the polarization of the Fe−N_ε bond is related to the bond strength. Thus, the details of the charge set most likely have a crucial impact on whether a bond is actually formed in the simulation. Figure 10 shows the result of a simulation based on imidazolate and ferric heme parameters, consistent with the hypothesis that H55 can move into a bonding conformation without significant distortion of the

dx.doi.org/10.1021/bi201368u | Biochemistry 2011, 50, 9664−9680

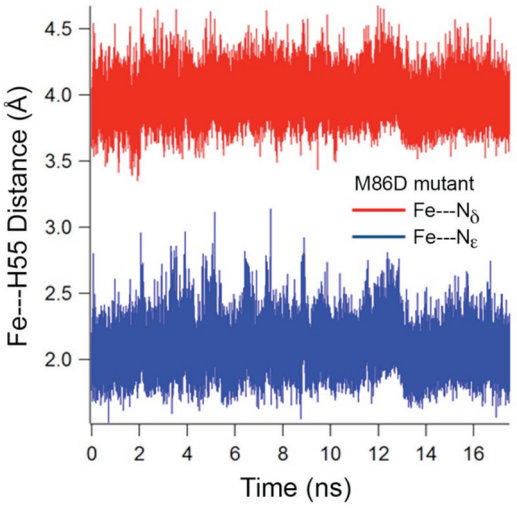

Figure 10. Molecular dynamics simulation of the M86D mutant Fe–N_δ (red) and Fe–N_ε (blue) distances with a charge set for the heme that accounts for ferric heme.

polypeptide backbone. The MD simulation is also intended to show that a realistic charge set will give rise to the hexacoordinate species that serves as a model for hemichrome. However, if the MD simulations and DFT calculations are taken together, they suggest that the imidazolate form of the distal histidine will form a stronger bond and, possibly, that the imidazolate form is essential for bonding.

The orientation of the proximal histidine, H89, and the position of the amino acid in position 86 were also monitored on the basis of the MD simulations. The calculated NA–Fe–N_ε–C_ε dihedral angles are −45.7 ± 9.2° and −40.7 ± 9.0° in M86E and M86D, respectively, where NA is one of the pyrrole nitrogens and C_ε is the carbon between the N_δ and N_ε atoms. From Figure S5 of the Supporting Information, one can see that the aspartate of M86D is significantly closer to the H89 N_δ atom compared to glutamate 86 of the M86E mutant. For the M86D mutant, the average distances from the D86 carboxylate oxygen atoms to the H89 N_δ atom are 4.89 ± 0.69 and 4.98 ± 0.70 Å, respectively. For the M86E mutant, the average distances from the E86 carboxylate oxygen atoms to the H89 N_δ atom are 6.24 ± 0.46 and 6.03 ± 0.60 Å, respectively. The fluctuations of the aspartate and the glutamate residues are similar, consisting mainly of a rotation about the carboxylate carbon so that the O1 and O2 atoms are exchanged. This is the major dynamic motion observed in Figure S5 of the Supporting Information. The distance from the L83 carbonyl oxygen to the H89 N_δ atom is 3.05 ± 0.25 and 2.91 ± 0.16 Å in M86E and M86D, respectively.

The distance from the H55 N_δ and N_ε atoms to the heme Fe is plotted in Figure S6 of the Supporting Information. During the first 20 ns of the simulation, the average Fe–(H55)N_ε distance is 7.05 ± 0.67 and 6.67 ± 0.55 Å for M86E and M86D, respectively. The Fe–(H89)N_δ distances are significantly shorter in M86E and M86D: 5.60 ± 0.90 and 5.15 ± 0.69 Å, respectively.

DISCUSSION

As determined by the X-ray crystal structure of M86D-CN, the mutagenic replacement of M86 with an aspartate residue leads to a proximal structure that is comparable to the Asp-His-Fe triad found in CcP[14] (Figure 1). The effect of introducing this triad into a globin has prompted the investigation of its reactivity and ligation states in this study. While the initial goal had been to gain insight into how an increased push effect in a 3/3 globin could modulate the O–O bond cleavage rate of an Fe-bound H_2O_2 molecule, it was found instead that an internal competing effect, presumably caused by the distal histidine, appears to dominate the reactivity. Although an Asp-His-Fe triad was successfully installed for the M86D mutant, it functions with significantly less peroxidase activity than wild-type DHP A. On one hand, the mutation shifts the redox potential to a lower value, thus favoring the Fe(III) redox state of a typical peroxidase. On the other hand, the Fe(III) resting state of the M86D mutant was determined to be a 6cLS species at pH 7.0, which led us to investigate the possible origins of the ligation. Clearly, ligation by the distal histidine interferes with H_2O_2 binding, and thus, the data are consistent in providing inhibition of peroxidase activity in the M86D mutant. We studied the data from the viewpoints that (i) the distal histidine occupies the sixth ligand position or (ii) a solvent molecule is the sixth ligand but is strongly hydrogen bonded to the distal histidine. Either of these cases would increase the K_M for H_2O_2 significantly relative to DHP A on the basis of both steady state assays and stopped-flow kinetics experiments.

Significance of the M86 Residue in Wild-Type DHP A. As a baseline for comparison, wild-type DHP A has been shown to be a typical globin in this study as far as the ligation to the heme Fe is concerned. In Figure 6A, DHP A, HHMb, and HRP were examined for their ^{13}C resonances of a heme Fe-bound ^{13}C- and ^{15}N-labeled cyanide ligand. These NMR spectroscopic results reveal that the metcyano forms of DHP A and HHMb are consistent with their proximal histidines having neutral character, whereas ferric HRP-^{13}CN exhibits a proximal histidine with anionic character. Peroxidase resonances are typically observed at approximately −3500 ppm, whereas globins are observed further upfield at approximately −4200 ppm. This difference has been attributed to the anionic versus neutral character exhibited by the proximal histidine.[15,57] Because the DHP A-^{13}CN resonance falls at −4211 ppm at pH 7.0, we conclude that the proximal histidine is similar to globins and thus has neutral character.

It was previously hypothesized[3] that the M86 residue may have a role in contributing to a push effect in DHP A via one of the lone pairs of the sulfur atom, which could interact with H89 by charge transfer. Replacement of M86 with alanine, which removes this possible interaction, provides a test for this hypothesis. Finding that the M86A mutation gives rise to only a minor change in the ^{13}C NMR properties (Figure 6B), we conclude that M86 does not have a significant role in controlling the electronic state of the proximal histidine in DHP A.

Structural Characterization of M86D-CN and M86E-CN. The concept of installing a negatively charged amino acid into a globin to create a catalytic triad has led to a number of studies of the proximal region site-directed mutants.[25−28] Hydrogen bonding in native globins encompasses relatively weak interactions with the backbone carbonyl group or the hydroxyl group of a neighboring serine (i.e., S92 in HHMb and SWMb). The interaction may also involve a bifurcated hydrogen bond to both S92 and a backbone carbonyl. Attempts to establish an Asp-His-Fe catalytic triad in HHMb via mutation (e.g., the S92D variant) did not lead to the formation of this charge relay. In this crystal structure (PDB entry 1RSE),[25] a histidine side chain (H97) hydrogen bonds to a

dx.doi.org/10.1021/bi201368u | Biochemistry 2011, 50, 9664–9680

heme propionate that helps keep the heme propionate positioned in the proximal region, which may affect the stabilization of negative charge near the proximal histidine. The proximal structure of DHP A lacks the histidine residue that would structurally align with H97 in HHMb. Because H97 can interact with a heme propionate side chain, the presence of the carboxylate in this region thwarts any attempt to place a negative charge near H93 to create a charge relay. Consequently, the D92 residue (in the S92D mutant of mammalian globins) is displaced by the heme propionate and oriented toward the solution, rather than being positioned in the vicinity of the proximal histidine.

The origin of the close $(D86)O_{\delta}-(H89)N_{\delta}$ separation in M86D can be understood on the basis of the X-ray crystal structures of the metcyano forms of the M86D and M86E mutants. While the position of aspartate relative to H89 is favorable in M86D, the longer side chain of glutamate relative to aspartate appears to disrupt the close interaction. In the M86E mutant, the glutamate side chain is oriented toward the solvent and thus away from the proximal histidine, H89. The structure of M86D provides greater flexibility for the negatively charged aspartate relative to S92D of human myoglobin where the side chain is immediately adjacent to the proximal histidine, H93.

In addition to the positioning of the aspartate, the charge relay may be disrupted by reorientation of other amino acid residues on the proximal side. One possible structural feature that may protect the charge relay is the presence of a glutamine side chain (Q88) that may obstruct the positioning of a heme propionate group in DHP A, thus preventing one of the destabilizing interactions observed in HHMb and SWMb. As a result, the D86 side chain is attracted to N_{δ} of H89 and forms the Asp−His interaction. In summary, the structure of the DHP A proximal pocket permits a different outcome from mammalian myoglobins when a negatively charged residue is introduced near the proximal histidine (H89 in DHP A) because of the orientation of the heme propionates and the possible local conformation that positions a residue at precisely the correct distance for hydrogen bonding, i.e., aspartate rather than glutamate.

Functional Characterization of M86D and the Role of the Asp-His-Fe Triad. The impact of the M86D mutation on the redox and electronic properties of DHP A was evaluated using electrochemistry and ^{13}C paramagnetic NMR spectroscopy of the Fe(III)-^{13}CN species. The formal reduction potential observed for M86D [$E^{\circ\prime}$ = 76 ± 5 mV (Table 2)] is shifted ∼125 mV in a negative direction with respect to that of DHP A ($E^{\circ\prime}$ = 202 ± 6 mV).[63] This shift in potential is most likely a reflection of changes in two Gibbs free energy terms,[64] namely, solvent-restricted internal electrostatic interactions (ΔG_{int}) and Fe bonding interactions (ΔG_{cen}). A change in ΔG_{int} (i.e., $\Delta\Delta G_{int}$) will arise whenever a mutation results in an altered electrostatic interaction between the redox center and a buried charge within the protein interior, whereas a change in ΔG_{cen} (i.e., $\Delta\Delta G_{cen}$) will reflect an alteration of bonding interactions at the redox center.[63−65] Considering ΔG_{int} first, we note that M86 resides near the heme Fe and is a neutral amino acid. Replacement of M86 with a negatively charged residue such as aspartate would be predicted to cause a negative shift in reduction potential on the basis of charge stabilization.[66] The net charge of the porphyrin in the Fe(III) oxidation state is +1 (excluding any charge contribution from the heme propionates). Thus, introduction of a buried negative charge in the vicinity of the heme could electrostatically stabilize the Fe(III) state with respect to the uncharged Fe(II) state, leading to an expected lowering of the reduction potential.

Although it is logical to surmise that electrostatic stabilization contributes to the positive shift in reduction potential for M86D relative to that of wild-type DHP A, the magnitude of such a contribution is unclear. In an investigation of C*c*P D235 mutations, for example, Goodin and McRee[14] concluded that changes in iron bonding interactions (ΔG_{cen}) exerted a greater influence on the reduction potential of C*c*P than the mere presence or absence of a charge that is ∼6−7 Å from the heme Fe. The reduction potential of wild-type C*c*P is −183 mV, which is typical of a peroxidase. Upon replacement of D235 with alanine, which removes the negative charge and disrupts the Asp−His charge relay interaction, a positive shift of 105 mV in reduction potential was observed. On the other hand, replacing D235 with glutamate gave rise to the D235E mutant in which an internal negative charge [confirmed by solvent accessibility calculations[67] (see Supporting Information)] is retained at a similar distance (although not exactly at the same location) from the heme Fe as the aspartate negative charge in wild-type C*c*P (Fe−O separation of ∼6.6−7.1 Å). Despite the retention of an internal negative charge at a similar distance, C*c*P D235E experienced a positive shift in reduction potential of 70 mV, which comprises two-thirds of the shift magnitude observed for C*c*P D235A. To rationalize these observations, Goodin and McRee proposed a mechanism for redox control based predominantly on metal−ligand covalency modulated by the nature of hydrogen bonding between the proximal histidine and D235. The strong hydrogen bonding that exists in the wild-type form strengthens the Fe−N bond and gives rise to increased metal−ligand covalency. In the case of C*c*P D235E, it was proposed that poorer hydrogen bonding due to non-optimal interaction angles resulted in a decrease in metal−ligand covalency. For DHP A, the ^{13}C paramagnetic NMR results (Table 2), the negative shift in reduction potential (Table 2), and trends in Mulliken charges in the DFT calculations (Table 4) are all consistent with increased metal−ligand covalency in the M86D mutant.

To aid in the characterization of an Asp-His-Fe triad in the M86D mutant of DHP A, ^{13}C paramagnetic NMR spectroscopy of Fe(III)-bound $^{13}C^{15}N$ was undertaken because of the ability to probe the push effect.[15,57,68,69] The ^{13}C resonance of the bound cyanide will be considerably different for a histidine-ligated heme protein that has neutral histidine-like character versus one having histidinate-like character. Resonances for peroxidases and globins have been observed from −3500 to −4200 ppm with respect to TMS.[15,57] The globin family generally has values found in the far upfield region (−4200 ppm), while peroxidase values are generally found ∼700 ppm further downfield (−3500 ppm). It was recently shown[15] that the disruption of the Asp-His-Fe triad in C*c*P in proximal region mutants C*c*P D235N and C*c*P D235A gave rise to upfield shifts of −151 and −221 ppm, respectively, relative to the wild-type protein. Nonaka et al.[15] speculated that because a large ^{13}C NMR chemical shift range between globins and peroxidases persists even when the Asp-His-Fe triad is removed in C*c*P, peroxidases may have a stronger intrinsic push effect than globins based on the differential location of the proximal histidine in these two families of proteins.

Table 2 shows M86D to be shifted +131 ppm downfield from DHP A, which indicates that the presence of D86 gives rise to more electron density on the heme Fe (stronger push

effect), although certainly not to the extent that is observed in heme peroxidases in the C*c*P superfamily. This result is consistent with the proximal region C*c*P mutants in the study by Nonaka et al.[15] in two respects, namely, shift direction and magnitude. The direction of the ^{13}C NMR shift in M86D, into which a proximal triad has been introduced, is opposite to the shifts observed in the C*c*P mutants from which the triad had been deleted. Furthermore, the magnitudes of the shifts observed as a result of the DHP A and C*c*P mutations are roughly comparable.

The Asp-His-Fe Triad of M86D Results in a 6cLS Species That Is Inhibitory with Respect to H_2O_2 Binding and Activation. The presence of the Asp-His-Fe triad in M86D has a deleterious effect on the reaction with H_2O_2 under physiological conditions. Stopped-flow kinetic measurements failed to detect an ferryl intermediate at low H_2O_2 concentrations. Because cyanide was required to stabilize the protein for X-ray crystallography, we cannot provide a further structural model for this inhibition based on the crystal structure. However, the UV−visible spectroscopic data clearly establish the formation of a 6cLS species even when cyanide is not present (Figure S3 of the Supporting Information). At pH 7.0, the M86D resonance Raman spectrum (Figure 8) is consistent with a 6cLS species. This observation is consistent with the distal histidine binding as a sixth ligand to the heme Fe in the Fe(III) oxidation state, which is also known as ferric hemichrome. M86D has a resonance Raman spectrum similar to that of the ferric hemichrome observed for the C*c*P H181G mutant.[60] The ν_3, ν_2, $\nu_{C=C}$, and ν_{10} modes are all characteristic of a bis-histidyl complex. Furthermore, the ν_{28} and ν_{38} modes observed in bis-histidyl 6cLS model compounds[59] are present in the M86D spectrum, as well (Figure 8A). The MD simulations show that the protein conformation required to form the ferric hemichrome is within the thermal energy of the pentacoordinate form. Figure 10 shows the results of a simulation with a charge set that mimics ferric heme. The N_ε atom of H55 is within bonding distance of the heme Fe, consistent with the formation of a hexacoordinate hemichrome conformation. The MD simulations also reveal that the hexacoordinate bis-histidine adduct is favored only for the charge set corresponding to the imidazole for H55 and for ferric heme and not with the ferrous heme charge set. Thus, the MD simulations are consistent with the lack of formation of ferrous hemochrome.

Although our data favor the formation of a hemichrome adduct, the 6cLS resonance Raman observation could originate from a strongly hydrogen bonded solvent molecule situated between the heme Fe and H55. This viewpoint is reasonable with respect to the wild-type DHP A X-ray crystal structure of the closed conformation (PDB entry 2QFK) because the shortest H55(N_ε)−Fe distance is 4.5 Å. Despite this possibility, it should be noted that in a previous study by Smulevich et al.,[60] the hydroxide anion sixth ligand in various heme proteins exhibits α/β bands in the UV−vis spectrum that differed significantly in wavelength maxima from the α/β bands of the C*c*P H181G mutant. The wavelength maxima for the α/β bands of M86D are consistent with those of C*c*P H181G, which strengthens the argument against there being a strongly hydrogen bonded solvent molecule bound to the heme iron.

CONCLUSIONS

We have shown that the proximal side of DHP A is sufficiently polar to tolerate a buried negative charge when the M86 residue is replaced with aspartate (M86D). Consequently, the M86D mutant forms a charge relay, Asp-His-Fe, observed for the first time in an X-ray crystal structure of a globin. On the other hand, the M86E mutant does not form a structure with the negative charge of glutamate buried inside the protein. Instead, this glutamate rearranges toward the solvent much the same way that aspartate is positioned in the myoglobin S92D mutant.[25,26] The subtle difference between the structures is dependent upon the ability of the carboxyl group to orient so that it can simultaneously interact with the H89 $N_\delta H$ group and with solvent, in M86D. The lack of a histidine parallel to the heme plane (e.g., H97 in SWMb) and a fortuitous positioning of Q88 in DHP A appear to prevent interference with the charge relay by reorientation of the heme propionate in the proximal region.

This study brings forth evidence that the charge relay found in peroxidases is involved in a mechanism for tuning the redox potential of the heme. We base this conclusion on X-ray crystal structure data showing that a globin with the 3/3 α-helical fold can support an Asp-His-Fe triad installed by site-directed mutagenesis. The M86D mutant of DHP A has the structural features of a charge relay, with a strong hydrogen bonding interaction between an aspartate oxygen and the proximal histidine N_δ atom. On the other hand, the glutamate carboxylate group in M86E is solvent-exposed, which leads to a significantly weaker interaction. Consistent with this structural observation, the redox and kinetic effects of the M86D mutant are significantly greater than those for the M86E mutant, whereas the control M86A mutant shows modest effects on these properties compared to those of wild-type DHP A. The slow turnover observed in the M86D mutant is due to the formation of a 6cLS species in the Fe(III) oxidation state observed by both UV−vis and resonance Raman spectroscopies. The data do not prove the identity of the sixth ligand in the 6cLS species, but either H55 or a strongly bound water molecule may bind as the sixth ligand to the heme Fe. However, in either case, this ligand acts as a strong peroxidase inhibitor with respect to the binding of cosubstrate H_2O_2, which is caused by the trans effect. The study further clarifies why the N_ε atom of the distal histidine in peroxidases is generally found between 5.5 and 6.0 Å from the heme Fe,[8] which is approximately 1.0−1.5 Å farther than in most globins. This positioning appears to be strategic for two main reasons. (1) The longer distance from the heme Fe aids in precluding the formation of a ferric 6cLS species, and (2) the distal histidine in peroxidases can act as an acid/base catalyst. The distal histidines in mammalian globins have their N_ε atom positioned much closer to the heme Fe (between 4.1 and 4.6 Å), which stabilizes oxygen binding and discriminates against carbon monoxide binding; however, this conformation does not lead to optimal peroxidase activity. The charge relay is not essential for peroxidase activity and indeed presents a structural problem for peroxidase function because an increase in positive charge on the heme Fe has a trans effect that can lead to the ligation of the distal histidine or a solvent molecule. Instead, the charge relay is most likely the redox tuning mechanism that permits peroxidases to have a range of functions. Consistent with this hypothesis, DHP A is a functioning peroxidase, with the highest redox potential of any known peroxidase and a complete lack of a charge relay.

ASSOCIATED CONTENT

Supporting Information

Protocols for the purification of horse heart myoglobin (HHMb) and horseradish peroxidase (HRP type I), reduction potentials, solvent accessibility areas, and atomic distances for peroxidases and 3/3 globins (Table S1), charge sets for ferric and ferrous heme used in the MD simulations (Table S2), charge sets for neutral imidazole and anionic imidazolate used in the MD simulations (Table S3), distances (angstroms) for Fe−N separations of neutral imidazole and anionic imidazolate used in the MD simulations (Table S4), single-mixing stopped-flow kinetics of the M86A mutant with H_2O_2 (Figure S1), single-mixing stopped-flow kinetics of the DHP A M86A mutant with hydrogen peroxide (Figure S2), UV−vis spectra of M86D in the presence and absence of cyanide ion (Figure S3), heme Fe−H55 nitrogen distances from MD simulations of ferric DHP A M86D and M86E with neutral histidine (Figure S4), distances from the oxygen atoms of glutamate and aspartate to the N_δ atom of H89 from molecular dynamics simulations (Figure S5), and distances between the nitrogen atoms (N_δ and N_ε) of H55 and the heme Fe from MD simulations (Figure S6). This material is available free of charge via the Internet at http://pubs.acs.org.

Accession Codes

The atomic coordinates and structure factors of the dehaloperoxidase A mutants M86E and M86D have been deposited in the Protein Data Bank as entries 3MYM and 3MYN, respectively.

AUTHOR INFORMATION

Corresponding Author

*E.F.B.: telephone, (919) 515-7069; e-mail, efbowden@ncsu.edu. S.F.: telephone, (919) 515-8915; fax, (919) 515-8920; e-mail, stefan_franzen@ncsu.edu.

Funding

This project was supported by Army Research Office Grants 51432-CH-SR (E.F.B.) and 57861-LS (S.F. and R.A.G.) and by the North Carolina State University Molecular Biotechnology Training Program through a National Institutes of Health T32 Biotechnology Traineeship grant (J.D.).

ACKNOWLEDGMENTS

We thank Professor Giulietta Smulevich and Dr. Sarah E. J. Bowman for insightful discussions.

ABBREVIATIONS

DHP A, dehaloperoxidase-hemoglobin A; M86E, M86D, and M86A, DHP A mutants; M86D-CN, M86D with CN^- ion bound; Cpd ES, Compound ES; Cpd II, Compound II; TXP, 2,4,6-trihalophenolate; DXQ, 2,6-dihaloquinone; 5cHS, pentacoordinate high-spin; 6cLS, hexacoordinate low-spin; HHMb, horse heart myoglobin; SWMb, sperm whale myoglobin; HRP, horseradish peroxidase; C*c*P, cytochrome *c* peroxidase; SEC, spectroelectrochemistry; MD, molecular dynamics; DFT, density functional theory; 4-MeIm, 4-methylimidazole; KPB, potassium phosphate buffer; Im_{distal}, imidazole on the distal side; $Im_{proximal}$, imidazole on the proximal side.

REFERENCES

(1) Chen, Y. P., Woodin, S. A., Lincoln, D. E., and Lovell, C. R. (1996) An unusual dehalogenating peroxidase from the marine terebellid polychaete *Amphitrite ornata*. *J. Biol. Chem. 271*, 4609−4612.

(2) Lebioda, L., LaCount, M. W., Zhang, E., Chen, Y. P., Han, K. P., Whitton, M. M., Lincoln, D. E., and Woodin, S. A. (1999) An enzymatic globin from a marine worm. *Nature 401*, 445.

(3) LaCount, M. W., Zhang, E. L., Chen, Y. P., Han, K. P., Whitton, M. M., Lincoln, D. E., Woodin, S. A., and Lebioda, L. (2000) The crystal structure and amino acid sequence of dehaloperoxidase from *Amphitrite ornata* indicate common ancestry with globins. *J. Biol. Chem. 275*, 18712−18716.

(4) Belyea, J., Gilvey, L. B., Davis, M. F., Godek, M., Sit, T. L., Lommel, S. A., and Franzen, S. (2005) Enzyme function of the globin dehaloperoxidase from *Amphitrite ornata* is activated by substrate binding. *Biochemistry 44*, 15637−15644.

(5) Bashford, D., Chothia, C., and Lesk, A. M. (1987) Determinants of a protein fold: Unique features of the globin amino-acid-sequences. *J. Mol. Biol. 196*, 199−216.

(6) Vinogradov, S. N., Hoogewijs, D., Bailly, X., Arredondo-Peter, R., Gough, J., Dewilde, S., Moens, L., and Vanfleteren, J. R. (2006) A phylogenomic profile of globins. *BMC Evol. Biol. 6*, 31.

(7) Poulos, T. L., and Kraut, J. (1980) The stereochemistry of peroxidase catalysis. *J. Biol. Chem. 255*, 8199−8205.

(8) Matsui, T., Ozaki, S., Liong, E., Phillips, G. N. Jr., and Watanabe, Y. (1999) Effects of the location of distal histidine in the reaction of myoglobin with hydrogen peroxide. *J. Biol. Chem. 274*, 2838−2844.

(9) Redaelli, C., Monzani, E., Santagostini, L., Casella, L., Sanangelantoni, A. M., Pierattelli, R., and Banci, L. (2002) Characterization and peroxidase activity of a myoglobin mutant containing a distal arginine. *ChemBioChem 3*, 226−233.

(10) Davydov, R., Osborne, R. L., Shanmugam, M., Du, J., Dawson, J. H., and Hoffman, B. M. (2010) Probing the oxyferrous and catalytically active ferryl states of *Amphitrite ornata* dehaloperoxidase by cryoreduction and EPR/ENDOR spectroscopy. Detection of compound I. *J. Am. Chem. Soc. 132*, 14995−15004.

(11) Feducia, J., Dumarieh, R., Gilvey, L. B. G., Smirnova, T., Franzen, S., and Ghiladi, R. A. (2009) Characterization of dehaloperoxidase compound ES and its reactivity with trihalophenols. *Biochemistry 48*, 995−1005.

(12) D'Antonio, J., D'Antonio, E. L., Thompson, M. K., Bowden, E. F., Franzen, S., Smirnova, T., and Ghiladi, R. A. (2010) Spectroscopic and mechanistic investigations of dehaloperoxidase B from *Amphitrite ornata*. *Biochemistry 49*, 6600−6616.

(13) Dawson, J. H. (1988) Probing structure-function relations in heme-containing oxygenases and peroxidases. *Science 240*, 433−439.

(14) Goodin, D. B., and McRee, D. E. (1993) The Asp-His-Fe triad of cytochrome c peroxidase controls the reduction potential, electronic structure, and coupling of the tryptophan free radical to the heme. *Biochemistry 32*, 3313−3324.

(15) Nonaka, D., Wariishi, H., Welinder, K. G., and Fujii, H. (2010) Paramagnetic ^{13}C and ^{15}N NMR analyses of the push and pull effects in cytochrome c peroxidase and *Coprinus cinereus* peroxidase variants: Functional roles of highly conserved amino acids around heme. *Biochemistry 49*, 49−57.

(16) Poulos, T. L. (1996) The role of the proximal ligand in heme enzymes. *J. Biol. Inorg. Chem. 1*, 356−359.

(17) Hirst, J., Wilcox, S. K., Ai, J., Moenne-Loccoz, P., Loehr, T. M., and Goodin, D. B. (2001) Replacement of the axial histidine ligand with imidazole in cytochrome c peroxidase. 2. Effects on heme coordination and function. *Biochemistry 40*, 1274−1283.

(18) Bertini, I., Sigel, A., and Sigel, H., Eds. (2001) *Handbook on metalloproteins*, Chapter 9, pp 330, Marcel Dekker, Inc., New York.

(19) Ayala, M., Roman, R., and Vazquez-Duhalt, R. (2007) A catalytic approach to estimate the redox potential of heme-peroxidases. *Biochem. Biophys. Res. Commun. 357*, 804−808.

(20) Roach, M. P., Ozaki, S., and Watanabe, Y. (2000) Investigations of the myoglobin cavity mutant H93G with unnatural imidazole proximal ligands as a modular peroxide O-O bond cleavage model system. *Biochemistry 39*, 1446−1454.

(21) Erman, J. E., Vitello, L. B., Miller, M. A., and Kraut, J. (1992) Active-site mutations in cytochrome c peroxidase: A critical role for

histidine-52 in the rate of formation of compound I. *J. Am. Chem. Soc. 114*, 6592−6593.
(22) El Kasmi, A., Leopold, M. C., Galligan, R., Robertson, R. T., Saavedra, S. S., El Kacemi, K., and Bowden, E. F. (2002) Adsorptive immobilization of cytochrome c on indium/tin oxide (ITO): Electrochemical evidence for electron transfer-induced conformational changes. *Electrochem. Commun. 4*, 177−181.
(23) El Hammi, E., Warkentin, E., Demmer, U., Limam, F., Marzouki, N. M., Ermler, U., and Baciou, L. (2011) Structure of *Ralstonia eutropha* flavohemoglobin in complex with three antibiotic azole compounds. *Biochemistry 50*, 1255−1264.
(24) Mukai, M., Mills, C. E., Poole, R. K., and Yeh, S. R. (2001) Flavohemoglobin, a globin with a peroxidase-like catalytic site. *J. Biol. Chem. 276*, 7272−7277.
(25) Lloyd, E., Burk, D. L., Ferrer, J. C., Maurus, R., Doran, J., Carey, P. R., Brayer, G. D., and Mauk, A. G. (1996) Electrostatic modification of the active site of myoglobin: Characterization of the proximal Ser92Asp variant. *Biochemistry 35*, 11901−11912.
(26) Roncone, R., Monzani, E., Murtas, M., Battaini, G., Pennati, A., Sanangelanton, A. M., Zuccotti, S., Bolognesi, M., and Casella, L. (2004) Engineering peroxidase activity in myoglobin: The haem cavity structure and peroxide activation in the T67R/S92D mutant and its derivative reconstituted with protohaemin-L-histidine. *Biochem. J. 377*, 717−724.
(27) Sinclair, R., Hallam, S., Chen, M., Chance, B., and Powers, L. (1996) Active site structure in cytochrome c peroxidase and myoglobin mutants: Effects of altered hydrogen bonding to the proximal histidine. *Biochemistry 35*, 15120−15128.
(28) Shiro, Y., Iizuka, T., Marubayashi, K., Ogura, T., Kitagawa, T., Balasubramanian, S., and Boxer, S. G. (1994) Spectroscopic study of Ser92 mutants of human myoglobin: Hydrogen bonding effect of Ser92 to proximal His93 on structure and property of myoglobin. *Biochemistry 33*, 14986−14992.
(29) Franzen, S. (2001) Effect of a charge relay on the vibrational frequencies of carbonmonoxy iron porphine adducts: The coupling of changes in axial ligand bond strength and porphine core size. *J. Am. Chem. Soc. 123*, 12578−12589.
(30) Franzen, S., Roach, M. P., Chen, Y. P., Dyer, R. B., Woodruff, W. H., and Dawson, J. H. (1998) The unusual reactivities of *Amphirite ornata* dehaloperoxidase and *Notomastus lobatus* chloroperoxidase do not arise from a histidine imidazolate proximal heme iron ligand. *J. Am. Chem. Soc. 120*, 4658−4661.
(31) Meyer, T. J. (1967) Ph.D. Thesis, Stanford University, Stanford, CA.
(32) Smolenaers, P. J., and Beattie, J. K. (1979) Tris-(ethylenediamine)ruthenium(II) and tris(ethylenediamine)ruthenium-(III) complexes. *Inorg. Synth. 19*, 117−121.
(33) de Serrano, V. S., D'Antonio, J., Franzen, S., and Ghiladi, R. A. (2010) Structure of dehaloperoxidase B at 1.58 Å resolution and structural characterization of the ab dimer from *Amphitrite ornata*. *Acta Crystallogr. D66*, 529−538.
(34) de Serrano, V., Chen, Z. X., Davis, M. F., and Franzen, S. (2007) X-ray crystal structural analysis of the binding site in the ferric and oxyferrous forms of the recombinant heme dehaloperoxidase cloned from *Amphitrite ornata*. *Acta Crystallogr. D63*, 1094−1101.
(35) Shannon, L. M., Kay, E., and Lew, J. Y. (1966) Peroxidase isozymes from horseradish roots. I. Isolation and physical properties. *J. Biol. Chem. 241*, 2166−2172.
(36) Taniguchi, I., Watanabe, K., Tominaga, M., and Hawkridge, F. M. (1992) Direct electron transfer of horse heart myoglobin at an indium oxide electrode. *J. Electroanal. Chem. 333*, 331−338.
(37) Otwinowski, Z., and Minor, W. (1997) Processing of X-ray diffraction data collected in oscillation mode. *Methods Enzymol. 276*, 307−326.
(38) McCoy, A. J., Grosse-Kunstleve, R. W., Storoni, L. C., and Read, R. J. (2005) Likelihood-enhanced fast translation functions. *Acta Crystallogr. D61*, 458−464.
(39) Collaborative Computational Project, Number 4 (1994) The CCP4 suite: Programs for protein crystallography. *Acta Crystallogr. D50*, 760−763.
(40) Emsley, P., and Cowtan, K. (2004) Coot: Model-building tools for molecular graphics. *Acta Crystallogr. D60*, 2126−2132.
(41) Bowden, E. F., Cohen, D. J., and Hawkridge, F. M. (1982) Anaerobic thin-layer electrochemical-cell for planar optically transparent electrodes. *Anal. Chem. 54*, 1005−1008.
(42) Osborne, R. L., Surnithran, S., Coggins, M. K., Chen, Y. P., Lincoln, D. E., and Dawson, J. H. (2006) Spectroscopic characterization of the ferric states of *Amphitrite ornata* dehaloperoxidase and *Notomastus lobatus* chloroperoxidase: His-ligated peroxidases with globin-like proximal and distal properties. *J. Inorg. Biochem. 100*, 1100−1108.
(43) Phillips, J. C., Braun, R., Wang, W., Gumbart, J., Tajkhorshid, E., Villa, E., Chipot, C., Skeel, R. D., Kale, L., and Schulten, K. (2005) Scalable molecular dynamics with NAMD. *J. Comput. Chem. 26*, 1781−1802.
(44) Thompson, M. K., Franzen, S., Davis, M. F., Oliver, R. C., and Krueger, J. K. (2011) Dehaloperoxidase-hemoglobin from *Amphitrite ornata* is primarily a monomer in solution. *J. Phys. Chem. B 115*, 4266−4272.
(45) Humphrey, W., Dalke, A., and Schulten, K. (1996) VMD: Visual molecular dynamics. *J. Mol. Graphics 14*, 33−38.
(46) Becke, A. D. (1997) Density-functional thermochemistry. 5. Systematic optimization of exchange-correlation functionals. *J. Chem. Phys. 107*, 8554−8560.
(47) Lee, C. L., Yang, W., and Parr, R. G. (1988) Development of the Colle-Salvetti correlation-energy formula into a functional of the electron density. *Phys. Rev. B. 37*, 785−789.
(48) Delley, B. (1990) An all-electron numerical method for solving the local density functional for polyatomic molecules. *J. Chem. Phys. 92*, 508−517.
(49) Delley, B. (2000) From molecules to solids with the DMol(3) approach. *J. Chem. Phys. 113*, 7756−7764.
(50) Kohn, W., and Sham, L. J. (1965) Quantum density oscillations in an inhomogeneous electron gas. *Phys. Rev. A 137*, 1697−1699.
(51) Mermin, D. (1965) *Phys. Rev. A 137*, 1441−1443.
(52) Maiti, R., Van Domselaar, G. H., Zhang, H., and Wishart, D. S. (2004) SuperPose: A simple server for sophisticated structural superposition. *Nucleic Acids Res. 32*, W590−W594.
(53) DeAngelis, T. P., and Heineman, J. (1976) An electrochemical experiment using an optically transparent thin layer electrode. *J. Chem. Educ. 53*, 594−597.
(54) Veitch, N. C., Williams, R. J. P., Bone, N. M., Burke, J. F., and Smith, A. T. (1995) Solution characterization by NMR-spectroscopy of two horseradish-peroixdase isoenzyme-c mutants with alanine replacing either Phe142 or Phe143. *Eur. J. Biochem. 233*, 650−658.
(55) Emerson, S. D., and Lamar, G. N. (1990) Solution structural characterization of cyanometmyoglobin: Resonance assignment of heme cavity residues by 2-dimensional NMR. *Biochemistry 29*, 1545−1556.
(56) Davis, M. F., Gracz, H., Vendeix, F. A. P., de Serrano, V., Somasundaram, A., Decatur, S. M., and Franzen, S. (2009) Different modes of binding of mono-, di-, and trihalogenated phenols to the hemoglobin dehaloperoxidase from *Amphitrite ornata*. *Biochemistry 48*, 2164−2172.
(57) Fujii, H., and Yoshida, T. (2006) C-13 and N-15 NMR studies of iron-bound cyanides of heme proteins and related model complexes: Sensitive probe for detecting hydrogen-bonding interactions at the proximal and distal sides. *Inorg. Chem. 45*, 6816−6827.
(58) Dunford, H. B. (1999) *Heme Peroxidases*, Wiley-VCH, New York.
(59) Choi, S., Lee, J. J., Wei, Y. H., and Spiro, T. G. (1983) Resonance Raman and electronic spectra of heme a complexes and cytochrome oxidase. *J. Am. Chem. Soc. 105*, 3692−3707.
(60) Smulevich, G., Miller, M. A., Kraut, J., and Spiro, T. G. (1991) Conformational change and histidine control of heme chemistry in cytochrome c peroxidase: Resonance Raman evidence from Leu-52

and Gly-181 mutants of cytochrome c peroxidase. *Biochemistry 30*, 9546−9558.
(61) Belyea, J., Belyea, C. M., Lappi, S., and Franzen, S. (2006) Resonance Raman study of ferric heme adducts of dehaloperoxidase from *Amphitrite ornata*. *Biochemistry 45*, 14275−14284.
(62) Belyea, J., Belyea, C. M., Lappi, S., and Franzen, S. (2010) Correction to resonance Raman study of ferric heme adducts of dehaloperoxidase from *Amphitrite ornata*. *Biochemistry 49*, 1354.
(63) D'Antonio, E. L., Bowden, E. F., and Franzen, S. (2011) manuscript in preparation.
(64) Mauk, A. G., and Moore, G. R. (1997) Control of metalloprotein redox potentials: What does site-directed mutagenesis of hemoproteins tell us? *J. Biol. Inorg. Chem. 2*, 119−125.
(65) Moore, G. R., and Pettigrew, G. W. (1990) *Cytochromes c: Evolutionary, structural, and physicochemical aspects*, Springer-Verlag, Berlin.
(66) Varadarajan, R., Zewert, T. E., Gray, H. B., and Boxer, S. G. (1989) Effects of buried ionizable amino acids on the reduction potential of recombinant myoglobin. *Science 243*, 69−72.
(67) Hubbard, S. J., and Thornton, J. M. (1993) *NACCESS*, Department of Biochemistry and Molecular Biology, University College London, London.
(68) Fujii, H. (2002) C-13 NMR signal detection of iron-bound cyanide ions in ferric cyanide complexes of heme proteins. *J. Am. Chem. Soc. 124*, 5936−5937.
(69) Nonaka, D., Wariishi, H., and Fujii, H. (2009) Paramagnetic C-13 and N-15 NMR analyses of cyanide- ((CN)-C-13-N-15-) ligated ferric peroxidases: The push effect, not pull effect, modulates the compound I formation rate. *Biochemistry 48*, 898−905.
(70) Laskowski, R. A., MacArthur, M. W., Moss, D. S., and Thornton, J. M. (1993) PROCHECK: A program to check the stereochemical quality of protein structures. *J. Appl. Crystallogr. 26*, 283−291.